New Astronomy 111 (2024) 102235

Contents lists available at ScienceDirect

New Astronomy

journal homepage: www.elsevier.com/locate/newast

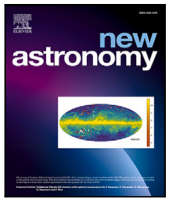

Resolving the pulsation contents of 13 δ Scuti stars with TESS and K2☆

Ai-Ying Zhou *

National Astronomical Observatories, Chinese Academy of Sciences, A20 Datun Road, Chaoyang District, Beijing, 100101, PR China
Key Laboratory of Radio Astronomy and Technology (Chinese Academy of Sciences), A20 Datun Road, Chaoyang District, Beijing, 100101, PR China

ARTICLE INFO

Keywords:
Stars: oscillation (pulsation)
Stars: variables: δ Scuti
γ Goradus
Techniques: photometric
Stars: individual: V1821 cyg
V2238 Cyg
BR Cnc
BU Cnc
BV Cnc
BN Cnc
EX Cnc
HD 73712
AD Ari
IT Dra
CD-54 7154
GSC 04040-01606

ABSTRACT

Using the *TESS* and *Kepler* K2 light curve archives, I have reanalyzed 13 known δ Scuti stars. AD Ari is now reclassified as a rotating ellipsoidal binary variable. EX Cnc and HD 73712 are reclassified as hybrid δ Sct-γ Dor pulsators. EX Cnc turns out to be an enticing asteroseismic target because of its three distinct groups of pulsation frequencies. The strong beating caused by two close frequencies is present in the star CD-54 7154. More than 71 pulsation frequencies were resolved for ι Boo and IT Dra with high significant levels, while V1821 Cyg, V2238 Cyg, BR Cnc, BU Cnc, and BV Cnc pulsate with a few dozen frequencies. In particular, K2 data revealed a significantly richer pulsational spectrum for the two δ Scuti stars BU Cnc and BV Cnc from six to 26. Unlike the other 12 stars, BN Cnc shows the simplest pulsation pattern. With high-precision and long-term space-based photometry, we are able to discern the pulsational contents of these stars more clearly and enhance our knowledge of them. This reanalysis using *TESS* and *Kepler* K2 data highlights the diversity of pulsational behavior among δ Scuti stars and the value of long-duration, high-precision photometry. Further asteroseismic modeling of these stars, particularly EX Cnc with its distinct frequency groups, promises to refine our understanding of their internal structures and pulsational mechanisms.

1. Introduction

The NASA's Transiting Exoplanet Survey Satellite (*TESS*, Ricker et al., 2015) data provide us with the best opportunity to study the light variations of a large number of stars with greater precision. Inspired by the detection of rich intrinsic pulsation content in the δ Scuti star HD 52788 (Zhou, 2024), we decided to expand our research to include more stars with the goal of resolving their detailed pulsational content.

Before using asteroseismology to probe the internal structures of stars by means of observed pulsation frequencies, one needs to identify the sequences of the pulsation modes in advance of comparing them with theoretically modeled modes. However, a large group of δ Scuti stars with rich pulsation spectra have not been systematically studied due to the fact that only a random subset of excited modes are observed in these stars, and the regular patterns are spoiled by rapid rotation (Bedding et al., 2020).

With the detection of regular sequences of pulsation modes in a star, a definitive mode identification can be reached. Recent work on the Pleiades cluster (Bedding et al., 2023) demonstrates the power of combining observations with *Gaia* (Gaia Collaboration et al., 2016a) and *TESS* for studying pulsating stars in open clusters. The large pulsational frequency separation and the frequency at maximum power can help constrain both the stellar evolution and structure models and oscillation models to better characterize the pulsating stars. Regularities in the frequency spectra benefit mode identification, and asteroseismic modeling can then be used to determine the age of their hosting clusters (Pamos Ortega et al., 2022, 2023). These advancements have encouraged the author to take advantage of space-based data to revisit well-classified known variables in stellar clusters.

This paper presents the pulsational frequency analyses of 13 selected δ Sct stars. It is aimed at resolving detailed pulsation content for each star, searching for any special frequency patterns, such as regular equal-spacing (Bedding et al., 2020; Gilliland et al., 2010), beating, resonance, and amplitude and/or phase modulations (Bowman et al., 2016; Buchler and Kolláth, 2011) for complementary consideration in mode identification.

Section 2 introduces the target sample and the light curve data used in this work. Section 3 outlines the analysis methods employed. Finally, Sections 4 and 5 present the results and conclusions of this work, respectively.

☆ This research is dedicated to my wife Jingyun Zhang who has been supporting my works all the time.

* Correspondence to: National Astronomical Observatories, Chinese Academy of Sciences, A20 Datun Road, Chaoyang District, Beijing, 100101, PR China.
E-mail address: aiying@nao.cas.cn.

https://doi.org/10.1016/j.newast.2024.102235
Received 7 December 2023; Received in revised form 31 March 2024; Accepted 11 April 2024
Available online 17 April 2024

Table 1
Sample of 13 selected known δ Sct stars.

Group	SN	TIC ID	Simbad main identification	Variability status
In clusters	01	TIC 90350726	NGC 6871: V1821 Cyg	DSCT
	02	TIC 41195917	NGC 6871: V2238 Cyg	DSCT
	03	TIC 307678320	NGC 2632: BR Cnc	DSCT
	04	TIC 175264749	NGC 2632: BU Cnc	DSCT
	05	TIC 175240124	NGC 2632: BV Cnc	DSCT
	06	TIC 175264756	NGC 2632: BN Cnc	DSCT
	07	TIC 175261925	NGC 2632: HD 73712	DSCT+SB+**GDOR**
	08	TIC 437039231	NGC 2682: EX Cnc	DSCT+**GDOR**
Field stars	09	TIC 246938869	AD Ari	DSCT → **ELL**
	10	TIC 310381204	ι Boo = HR 5350	DSCT+EB → **DSCT**
	11	TIC 166177270	IT Dra = SAO 16394	DSCT
	12	TIC 173503902	CD-54 7154	DSCT
	13	TIC 372724683	GSC 04040–01606	DSCT

2. The sample and data

2.1. Sample of targets

During the course of observing a known δ Sct star V1821 Cyg in the open cluster NGC 6871, one of the field star GSC 2683–3076 (=V2238 Cyg) was discovered to be a δ Sct star by our group (Du et al., 1999). Now we are going to revisit this field with *TESS*. NGC 2632, also known as Praesepe, is a young nearby open cluster (0.8 Gyr, 172 ± 47 pc). Here, we reviewed five of the δ Sct stars in NGC 2632 that were covered in the author's previous studies (e.g. Zhou et al., 2001c; Zhou, 2002), with the aim of deriving insights into the properties of stars using high-precision space photometry.

In addition, EX Cnc in NGC 2682 and five field stars were observed by the author. Finally, the author selected a set of 13 known δ Sct stars divided into two groups (Table 1):

- Eight known pulsating variable stars in the three young galactic open stellar clusters NGC 6871 (small, with 50–100 stars), NGC 2632 (larger, with ∼1000 stars), and NGC 2682. The former two are well known for their dense populations of δ Sct stars (about 15 and 12, respectively, according to Simbad). The NGC 2632 region was partly covered by the *Kepler* and *Kepler K2* missions.
- Five known field δ Sct stars that were previously observed by the author.

2.2. TESS data

The Transiting Exoplanet Survey Satellite (*TESS*, Ricker et al., 2015) is an MIT-led NASA mission dedicated to discovering transiting exoplanets orbiting nearby bright stars by an all-sky photometry survey. *TESS* rotates every ∼13.7 days per orbit, and it is equipped with four identical cameras with a combined field-of-view of 24° × 96° (known as an observing sector). A brief description of *TESS* was summarized in Zhou (2024). Readers can refer to the details in both the *TESS* Science Data Products Description Document[1] and the "Characteristics of the *TESS* space telescope" web page.[2]

The 16 CCDs on the *TESS* spacecraft actually take images and read them out continuously at 2-s intervals. However, the 2-s frames are processed on the spacecraft by the data handling unit (DHU), which stacks 2-s exposure images in groups of 60, 300 or 900 to produce 2-min, 10-min, and 30-min cadence images for general observations. The data on spacecraft are transmitted to Earth when the spacecraft reaches orbital perigee every ∼13.7 days. Each sector of the sky will be observed twice with a 27.4-day observing period, and there is a systematic gap of about half a day to one and a half days between two consecutive orbits. It is important to be aware of the timing structure involved in the spacecraft system and observation before conducting data analysis.

In addition, *TESS* produces additional pixels in small postage stamps surrounding a few bright asteroseismology targets and downloads them at a 20-s cadence (1000 stars). In July 2020, *TESS* began revisiting the sky in an extended ongoing mission that records full-frame images at a fast ten-minute cadence. *TESS* provides a golden opportunity for studying short to moderately long periodic variables, especially, δ Sct and γ Dor stars (Antoci et al., 2019), RR Lyr stars and so on.

To automate the process of checking the *TESS* archive at the MAST Portal (Mikulski Archive for Space Telescopes[3]), a Python program was written following the *TESS* Archive Manual,[4] using the ASTROPY and LIGHTKURVE packages (The Astropy Collaboration et al., 2018; Lightkurve Collaboration et al., 2018). The extracted light curves include: the NASA's Science Processing Operations Centre (SPOC) generated files and High Level Science Products (HLSP) for MAST-supported missions.[5]

The *TESS* Science Processing Operations Centre (SPOC) produces two kinds of light curves: Simple Aperture Photometry (SAP) and Presearch Data Conditioned Simple Aperture Photometry (PDCSAP). SAP flux is the flux after summing the calibrated pixels within the *TESS* optimal photometric aperture, while the PDCSAP is the SAP flux from which long-term trends have been removed using so-called Co-trending Basis Vectors and nominally corrected for instrumental variations and excessive scattered light. PDCSAP flux is usually cleaner data than the SAP flux and will have fewer systematic trends. Therefore, PDCSAP flux is widely used for final analysis without further processing (e.g. Dumusque et al., 2019; Demory et al., 2020; Battley et al., 2021). However, the PDCSAP flux might suffer from loss of long-term and transient burst variability being intrinsic to stars (Hill et al., 2022; Littlefield et al., 2021), so SAP flux is also used by some authors (e.g. von Essen et al., 2020; Steindl et al., 2021; Hon et al., 2021; Prša et al., 2022) accompanied with additional custom processing such as detrendings depending on science goals.

The fluxes (PDCSAP_Flux and SAP_Flux) are converted to magnitudes (PDCSAP_mag and SAP_mag) using the formula $mag = -2.5\log(Flux) + zeropoint$. The magnitude zero points 20.4436 and 20.2531 mag for converting SAP and PDCSAP fluxes into magnitudes, respectively were selected to match the $T_{\rm mag}$ of the *TESS* Input Catalog version 8.2 (TIC v8.2). Finally, a custom data processing of correction to severe systematic trends and artificial displacement of the two successive orbits' light curves is applied whenever needed. A full description of the data reduction is given in Zhou (2024).

2.3. Kepler K2 data

The *Kepler* second mission (*K2*, Howell et al., 2014) had released its data for open access.[6] Each *K2* Campaign has a duration of approximately 80 days. Light curve data are usually provided in a 30-min cadence. This long-time coverage improves the frequency resolution of variability detection and is suitable for both stable and unstable periodic and non-periodic variations of a wide range of variable star studies.

There are three main types of light curve data available to the public: (1) *K2* Systematics Correction (K2SC): This is a *K2* light curve detrending tool that uses Gaussian processes to robustly model the

[1] https://archive.stsci.edu/missions-and-data/tess.
[2] https://heasarc.gsfc.nasa.gov/docs/tess/the-tess-space-telescope.html.
[3] https://mast.stsci.edu/portal/Mashup/Clients/Mast/Portal.html; or https://archive.stsci.edu/tess/.
[4] The Beginner Tutorial Notebooks: https://outerspace.stsci.edu/display/TESS/TESS+Archive+Manual.
[5] https://archive.stsci.edu/hlsp.
[6] K2: Extending *Kepler*'s Power to the Ecliptic, The Ecliptic Plane Input Catalog (EPIC) for *Kepler*'s K2 mission, see http://keplerscience.arc.nasa.gov/K2/.

Table 2
Frequency solution of V1821 Cyg based on *TESS* sectors 14 and 15 in order of amplitude. The digits in parentheses represent the error in the last two or three decimal places. Amplitude units are milli-magnitudes (mmag), with typical uncertainties of 0.0483 mmag.

Frequency		Amplitude	Phase	SNR
(d^{-1})	(μHz)	(mmag)	(0-1)	
f_0 = 8.242804(99)	95.40	9.316	0.8514(16)	292.0
f_1 = 8.818414(678)	102.06	6.014	0.4022(106)	220.4
f_2 = 11.081546(266)	128.26	4.955	0.8659(41)	188.8
f_3 = 7.784887(244)	90.10	2.909	0.8084(38)	79.9
f_4 = 10.523831(366)	121.80	1.857	0.5910(57)	58.7
f_5 = 9.025902(367)	104.47	1.484	0.8562(57)	55.4
f_6 = 6.528729(368)	75.56	1.356	0.0249(57)	28.7
f_7 = 7.424097(421)	85.93	1.348	0.6054(66)	28.6
f_8 = 8.699668(456)	100.69	1.344	0.5155(71)	49.2
f_9 = 6.069261(383)	70.25	1.339	0.7659(60)	35.8
f_{10} = 6.605663(516)	76.45	1.286	0.5332(80)	27.2
f_{11} = 10.379898(557)	120.14	1.172	0.8938(87)	31.1
f_{12} = 11.231811(865)	130.00	1.081	0.6107(135)	41.2
f_{13} = 6.79021(179)	78.59	0.955	0.9006(279)	20.2
f_{14} = 11.334946(169)	131.19	0.885	0.4683(26)	33.7
f_{15} = 7.75810(93)	89.79	0.763	0.0358(144)	21.0
f_{16} = 9.03846(176)	104.61	0.727	0.3265(275)	27.1
f_{17} = 8.860836(751)	102.56	0.656	0.3702(117)	24.0
f_{18} = 9.751664(958)	112.87	0.570	0.1569(149)	16.8
f_{19} = 10.91737(108)	126.36	0.533	0.0851(169)	16.8
f_{20} = 9.58463(131)	110.93	0.514	0.4823(204)	15.1
f_{21} = 6.62731(101)	76.70	0.488	0.7725(157)	10.3
f_{22} = 9.79761(438)	113.40	0.456	0.3001(683)	13.4
f_{23} = 9.869381(72)	114.23	0.376	0.9901(11)	11.1
f_{24} = 11.03762(167)	127.75	0.279	0.3745(260)	10.6
f_{25} = 11.00491(242)	127.37	0.221	0.7026(377)	8.4
f_{26} = 11.55159(283)	133.70	0.204	0.2037(441)	5.9
f_{27} = 5.355046(332)	61.98	0.174	0.8965(52)	5.6
f_{28} = 13.84356(328)	160.23	0.151	0.2784(511)	4.8
Dependent frequencies within the frequency resolution 0.018518 d^{-1}:				
f_{29} = 7.77449(5) = f_3 − 0.0104	89.98	2.020	0.6311(08)	55.5
f_{30} = 7.78731(36) = f_3 − 0.0024	90.13	1.501	0.1968(57)	41.2
f_{31} = 8.8264(22) = f_1 + 0.0079	102.16	0.276	0.9438(348)	10.1
Zeropoint: −0.00000497 mag				
Residuals: 0.001678375 mag				

systematics due to the *Kepler* telescope pointing jitter together with the astrophysical variability. The K2SC-detrended light curves are especially suited for studying variable stars in *K2* photometry (by allowing us to remove the position-dependent systematics while keeping time-dependent variability intact), and searches for transiting planets (by allowing us to remove both the systematics and astrophysical variability). (2) *K2* Extracted Lightcurves (K2SFF): These light curves are extracted from the *K2* images using a variety of photometric apertures. They contain larger systematics than the original *Kepler* mission light curves, due to the reduction in pointing precision as a result of having to rely on only two reaction wheels. However, a technique has been developed to correct for the pointing-dependent nature of the pixel-level fluxes, which improves the photometric precision by typical factors of 2–5, and results in the median photometric performance of *K2* targets to within a factor of two of the original, 4-wheeled mission. (3) EVEREST light curves: These are products from an open-source pipeline for removing instrumental systematics from *K2* light curves, using a combination of pixel-level decorrelations to remove spacecraft pointing error and Gaussian processes to capture astrophysical variability. Light curves from campaigns 0 through 8, 102, 111, 112, 12, and 13 are currently available. Either K2SFF, K2SC, or EVEREST light curves can be used, depending on which one looks better. For our current work, we used K2SFF light curves. However, the K2SFF data is not yet flat, so we had to further remove a profile by fitting a polynomial of orders between 4 and 24 to the data. Each campaign dataset may be divided into 2 or 3 segments for better fitting and detrending. The residuals are then combined for pulsation analysis.

Table 3
Frequency solution of V2238 Cyg based on *TESS* Sectors 14 and 15. The digits in parentheses represent the error in the last two/three decimal places. Amplitude units are milli-magnitudes (mmag), with typical uncertainties of 0.1168 mmag.

Frequency (d^{-1})	μHz	Amplitude (mmag)	Phase (0-1)	SNR
f_0 = 15.706491(125)	181.79	9.528	0.3050(20)	59.9
f_1 = 9.506178(204)	110.03	5.838	0.2654(32)	56.2
f_2 = 8.003665(313)	92.64	3.803	0.9101(49)	42.6
f_3 = 13.006620(442)	150.54	2.693	0.1753(69)	20.8
f_4 = 7.393761(552)	85.58	2.158	0.4064(86)	19.2
f_5 = 13.698784(86)	158.55	13.805	0.8836(13)	108.9
f_6 = 16.653335(642)	192.75	1.857	0.8347(100)	17.2
f_7 = 12.375046(683)	143.23	1.744	0.6027(107)	18.1
f_8 = 13.957571(518)	161.55	2.300	0.6748(81)	18.1
f_9 = 14.779595(759)	171.06	1.569	0.3116(118)	12.9
f_{10} = 14.844955(837)	171.82	1.424	0.3430(130)	11.7
f_{11} = 15.068730(899)	174.41	1.325	0.3879(140)	8.7
f_{12} = 13.24527(174)	153.30	0.685	0.5473(271)	5.3
f_{13} = 12.92956(179)	149.65	0.665	0.2699(279)	5.1
f_{14} = 8.90253(188)	103.04	0.633	0.9442(293)	6.7
f_{15} = 10.11068(193)	117.02	0.618	0.9488(301)	6.3
f_{16} = 7.50853(167)	86.90	0.716	0.7601(260)	7.1
f_{17} = 11.52962(169)	133.44	0.707	0.4171(263)	8.3
f_{18} = 8.29477(255)	96.00	0.468	0.7138(397)	5.2
Dependent frequencies within the frequency resolution 0.018518 d^{-1}:				
f_{19} = f_5 + 0.00044	158.56	12.009	0.6419	94.7
f_{20} = f_0 − 0.00378	181.79	9.528	0.3050	59.9
f_{21} = f_3 − 0.0194	92.83	6.659	0.5853	74.5
Zeropoint: 9.99954193 mag				
Residuals: 0.0039986 mag				

2.4. Gaia and TIC v8.2 data

Both *Gaia* Data Release 3 (DR3, Gaia Collaboration et al., 2023, 2016a) and the *TESS* Input Catalog (TIC v8.2, Stassun et al., 2018; Paegert et al., 2021) are used to retrieve astronomical and stellar atmospheric parameters, including magnitudes in B and V, *Gaia* photometric magnitudes (G, BP, RP) and color indices ($BP-RP$, $G-RP$), parallax, distance, radius, radial velocity, effective temperature, luminosity, surface gravity, mass, etc. Absolute magnitude was calculated using the *Gaia* distance according to the definition $M_V = V + 5.0 - 5\log(d)$.

3. Frequency analysis

Fourier transform is a powerful tool for analyzing light curves to assist identification of light variability of a star. It is usually used to resolve light variations into a sum of multiple sine or cosine waveforms with different frequencies, amplitudes, and phases. We performed Fourier analysis of light curves using the PERIOD04 software package (Lenz and Breger, 2005). The procedure is the same as that described in Zhou (2024). We first performed a Fourier transform on the processed light curve. This analysis yields the amplitude spectrum, a graphical representation of the amplitude (intensity) of each frequency component present in the light curve. The amplitude spectrum reveals both the number of distinct frequencies contributing to the light variations and the strength (amplitude) of each frequency's contribution.

Next, we performed successive prewhitenings to pick up frequencies. This involves repeated subtraction of the best-fitting sine waves from the light curves and recalculating the Fourier transform on the residuals. The prewhitening process terminated when no significant peaks remain in the amplitude spectrum.

The frequency, amplitude and phase parameters of the best-fitting sine waves were then optimized using a least-squares fitting procedure. Finally, we recalculated the signal-to-noise ratio (SNR) based on the remained significant frequencies and residuals.

Particular attention was paid to aliasing and frequency resolution in resolving both lower and close frequencies. Aliasing is a phenomenon that can occur when the sampling rate of the data is not high enough to resolve all of the frequencies present in the signal. Frequency resolution is the ability to distinguish between two close frequencies.

4. Results for individual stars

4.1. NGC 6871

TESS observed this field and light curves are available at MAST in two products: the 2-min cadence SPOC (Sector 41) and 30-min cadence HLSP-QLP (Sectors 14 and 15).

The three sectors data, spanning from BJD 2458683.3628 to 2459446.5818 (during 2019-07-18 20:42 and 2021-08-20 01:57 UT), provide an effective frequency resolution of 0.012 d^{-1}, calculated by using the actual duration of observations (3 × 27.4 days). However, this value could be largely biased. The theoretic frequency resolution given by the reciprocal of the entire observing time span T, which is 763.2 days, would be $\Delta f = 1/T = 0.0013\ d^{-1}$, which is about ten times better than the effective frequency resolution. We will use the value $0.0013\ d^{-1}$ as the minimum resolvable frequency spacing between two close frequencies. This means that two frequencies with a difference less than $0.0013\ d^{-1}$ will be regarded as one term, otherwise they will be treated as two individual terms.

However, when combining the three sectors data for V1821 Cyg together, we found two strongest aliases at $a_1 = 0.054238\ d^{-1}$ and $a_2 = 47.998507\ d^{-1}$ with 20% and 11% intensity of the main peak, respectively. The first alias can be converted to an equivalent sampling gap of 18.437 days. The second alias a_2 is caused by the sampling intervals Δt of 30-min cadence data from Sectors 14 and 15, which have a Nyquist frequency of $24\ d^{-1}$ (i.e. the maximum possible frequency defined by $f_{max} = 1/(2\Delta t)$). Frequencies exceeding half the sampling rate would be aliases. The 2-min cadence (S0041) and 30-min cadence (S0014 and S0015) non-differential photometric data may have different amplitudes for a variable star. As the star's pulsational frequencies distribute in a narrow range of 5–15 d^{-1}, we prefer to apply Fourier analysis to the two sectors of 30-min cadence data (secured in BJD 2458683.3628–2458737.3853) in the frequency range 0–23 d^{-1}. Thus the actual frequency resolution becomes to be 0.0185 d^{-1}.

4.1.1. NGC 6871: V1821 Cyg

V1821 Cyg (=HD 227695 =TIC 90350726, $B = 10\overset{m}{.}56$, $V = 10\overset{m}{.}22$, A5p) is a known δ Sct star. We resolved 29 independent significant pulsational contents based on *TESS* data. This set of frequencies, reported in Table 2, is a great update to the previous solution of only two pulsation frequencies (Zhou et al., 2001a). Fig. 1 shows the typical *TESS* light curve in Sector 41 and the periodogram resulted from the two consecutive Sectors 14 and 15.

4.1.2. NGC 6871: V2238 Cyg

V2238 Cyg (= GSC 2683–3076 = TIC 41195917) was first revealed to be a δ Sct star by our group (Du et al., 1999). It was observed by *TESS* in sectors 14, 15, and 41. SPOC light curves are available with a cadence of 2 min for sector 41, while 30-min cadence HLSP-QLP data are available for sectors 14 and 15. Similar to that for V1821 Cyg, we resolved 19 individual pulsational frequency contents along with four dependent frequencies unresolvable by the effective frequency resolution based on the two consecutive *TESS* data in Sectors 14 and 15. The pulsational solution given in Table 3 greatly improves the previous detection of seven frequencies in the star's light variations (Zhou et al., 2001b). As seen in Fig. 2, the pulsations are in two distinct groups around 10 and 15, respectively.

Table 4
Frequency solution of BR Cnc based on *TESS* sectors 44 and 46. The digits in parentheses represent the error in the last two or three decimal places. Amplitude units are milli-magnitudes (mmag), with typical uncertainties of 0.0099 mmag.

Frequency (d^{-1})	μHz	Amplitude (mmag)	Phase (0-1)	SNR
f_0 = 24.978248(23)	289.10	3.054	0.8505(05)	77.4
f_1 = 11.464797(37)	132.69	1.870	0.0345(08)	87.1
f_2 = 8.202908(56)	94.94	1.238	0.5647(13)	50.7
f_3 = 12.784615(87)	147.97	0.801	0.2097(20)	41.1
f_4 = 10.364524(91)	119.96	0.761	0.2583(21)	36.4
f_5 = 10.971461(96)	126.98	0.723	0.0677(22)	34.5
f_6 = 24.185592(102)	279.93	0.683	0.2136(23)	17.3
f_7 = 11.744333(147)	135.93	0.474	0.1125(33)	22.1
f_8 = 15.790582(156)	182.76	0.444	0.2109(35)	22.0
f_9 = 5.393000(315)	62.42	0.220	0.8645(71)	12.7
f_{10} = 11.967700(237)	138.52	0.293	0.2289(54)	13.6
f_{11} = 12.893700(461)	149.23	0.151	0.5362(104)	7.7
f_{12} = 15.671600(485)	181.38	0.143	0.4780(110)	7.1
f_{13} = 16.227000(452)	187.81	0.153	0.5985(102)	10.4
f_{14} = 16.721100(60)	193.53	1.148	0.1667(14)	77.9
f_{15} = 19.869000(317)	229.97	0.219	0.9284(72)	13.6
f_{16} = 26.691000(212)	308.92	0.328	0.0215(48)	6.8
f_{17} = 39.315000(622)	455.03	0.111	0.4088(141)	5.4
f_{18} = 9.516344(176)	110.14	0.394	0.2545(40)	19.0
f_{19} = 2.607590(267)	30.18	0.260	0.2599(60)	14.5
f_{20} = 10.104400(384)	116.95	0.181	0.3809(87)	8.6
f_{21} = 14.309000(282)	165.61	0.246	0.2418(64)	12.0
f_{22} = 14.569000(545)	168.62	0.127	0.0507(123)	6.2
f_{23} = 15.678000(194)	181.46	0.357	0.5510(44)	17.7
f_{24} = 16.264000(777)	188.24	0.089	0.1790(176)	6.1
f_{25} = 17.144900(294)	198.44	0.236	0.1924(66)	17.8
f_{26} = 29.335000(327)	339.53	0.212	0.8914(74)	5.2
f_{27} = 30.411000(233)	351.98	0.298	0.9032(53)	8.6
f_{28} = 16.689820(181)	193.17	0.383	0.8279(41)	26.0
f_{29} = 30.321977(206)	350.95	0.337	0.4091(47)	9.7
f_{30} = 21.792000(310)	252.22	0.224	0.2281(70)	13.4
f_{31} = 30.365375(199)	351.45	0.348	0.5783(45)	10.0
Dependent frequencies within the frequency resolution 0.0118 d^{-1}				
$f_{32} = 2f_1 - 2f_4 + 0.005846$		0.1740	0.1210	14.5
$f_{33} = f_4 - f_2 + 0.002416$		0.1950	0.8253	10.8
$f_{34} = f_1 + f_3 - 0.000588$		0.4830	0.5953	12.2
$f_{35} = f_1 + f_3 - 0.003088$		0.2350	0.3234	6.0
Zeropoint: 8.52563615 mag				
Residuals: 0.0012473623 mag				

Table 5
TIC v8.2 catalog parameters for four neighboring δ Sct stars BU, BV, BN Cnc and HD 73712 in NGC 2632.

ID/Parameters	BU Cnc	BV Cnc	BN Cnc	HD 73712
HD	HD 73576	HD 73746	HD 73763	HD 73712
TIC	175240124	175264756	175264749	175261925
EPIC	211936696	211931309	211933524	211941583
RA	08 39 44.664	08 40 32.959	08 40 39.234	08 40 20.145
Dec	+19 16 30.77	+19 11 39.57	+19 13 41.85	+19 20 56.32
B	7.823	8.933	7.986	7.019
V	7.66791	8.66168	7.81068	6.78136
T_{eff}	7890.0	7333.36	7744.0	7408.0
SpType	A7Vn	F0V	A9V	A9V
log g	3.85145	4.11231	3.81905	3.30218
$M/M_\odot$	1.89	1.663	1.827	1.692
$R/R_\odot$	2.70108	1.8764	2.75664	4.81

4.2. NGC 2632

NGC 2632, also known as Praesepe, is a young nearby open cluster (0.8 Gyr, 172 ± 47 pc), it is well known for its dense population of 14 δ Sct stars in a small region. *TESS* observed the NGC 2632 region in Sectors 44 and 46 at the short cadence of 2 min, together with 10-min cadence QLP light curves in Sector 45. *Kepler* K2 observed the Praesepe cluster area during 2015.04.27–2018.07.02 in Campaigns c05, c16 and c18. Here, we reviewed five of the δ Sct stars in NGC 2632 that were covered in the author's previous studies, with the aim of

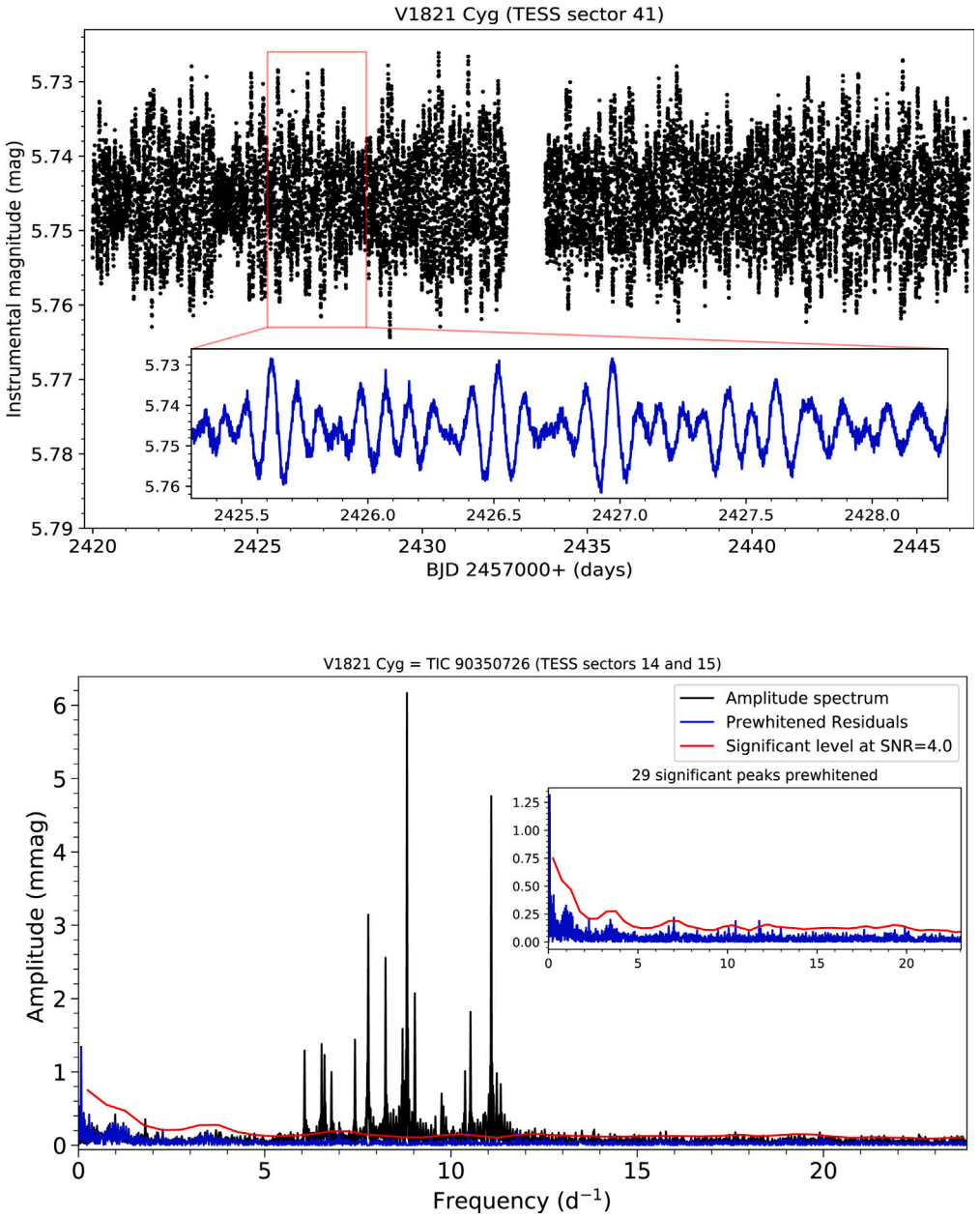

Fig. 1. *TESS* light curve of V1821 Cyg in Sector 41 (Top) and amplitude spectrum based on Sectors 14 and 15 with the inset showing the residuals (Bottom).

deriving insights into the properties of stars using high-precision space photometry.

4.2.1. NGC 2632: BR Cnc

BR Cnc (= HD 73175 = TIC 307678320, F0Vn, $V = 8^{m}.25$, $B = 8^{m}.48$) is one of the members of stellar cluster Praesepe (NGC 2632) and a known δ Sct star (Zhou et al., 2001c; Zhou, 2002). The Data Validation Report Summary produced in the *TESS* Science Processing Operations Center Pipeline (SPOC) presented a transit analysis with a period of 4.18766 ± 0.00109 days. However, it is finally not a *TESS* Objects of Interest (TOI, Guerrero et al., 2021), and the suspicion of hosting an exoplanet was not confirmed either by the NASA Exoplanet Catalog[7] or the NASA Exoplanet Archive (Exoplanet and Candidate Statistics) at Caltech.[8]

However, no *Kepler* data of BR Cnc available for public. Based on the short cadence light curves in *TESS* Sectors 44 and 46, an attentive pulsational frequency analysis yields 32 independent frequencies. These frequencies are resolved over the effective frequency resolution 0.0128 d^{-1}, derived from the observing duration (BJD 2459500.3616 to 2459578.7058). The results are presented in Table 4 and Fig. 3. These frequencies are distributed in two distinct groups around the two strongest frequencies at f_0 = 24.9782 and f_1 = 11.4648 d^{-1}, respectively.

4.2.2. NGC 2632: BU Cnc, BV Cnc, BN Cnc and HD 73712

BU Cnc, BN Cnc, BV Cnc and HD 73712 are four neighboring known δ Sct stars in the Praesepe cluster (NGC 2632). Fig. 4 shows their finder's chart and neighborhood. These four stars form a close-knit group approximately 40 arcminutes southeast of BR Cnc.

BU Cnc was once observed at five international observatories during a multi-site photoelectric photometry campaign during 1989 February

[7] https://exoplanets.nasa.gov/discovery/exoplanet-catalog/.
[8] https://exoplanetarchive.ipac.caltech.edu/docs/counts_detail.html.

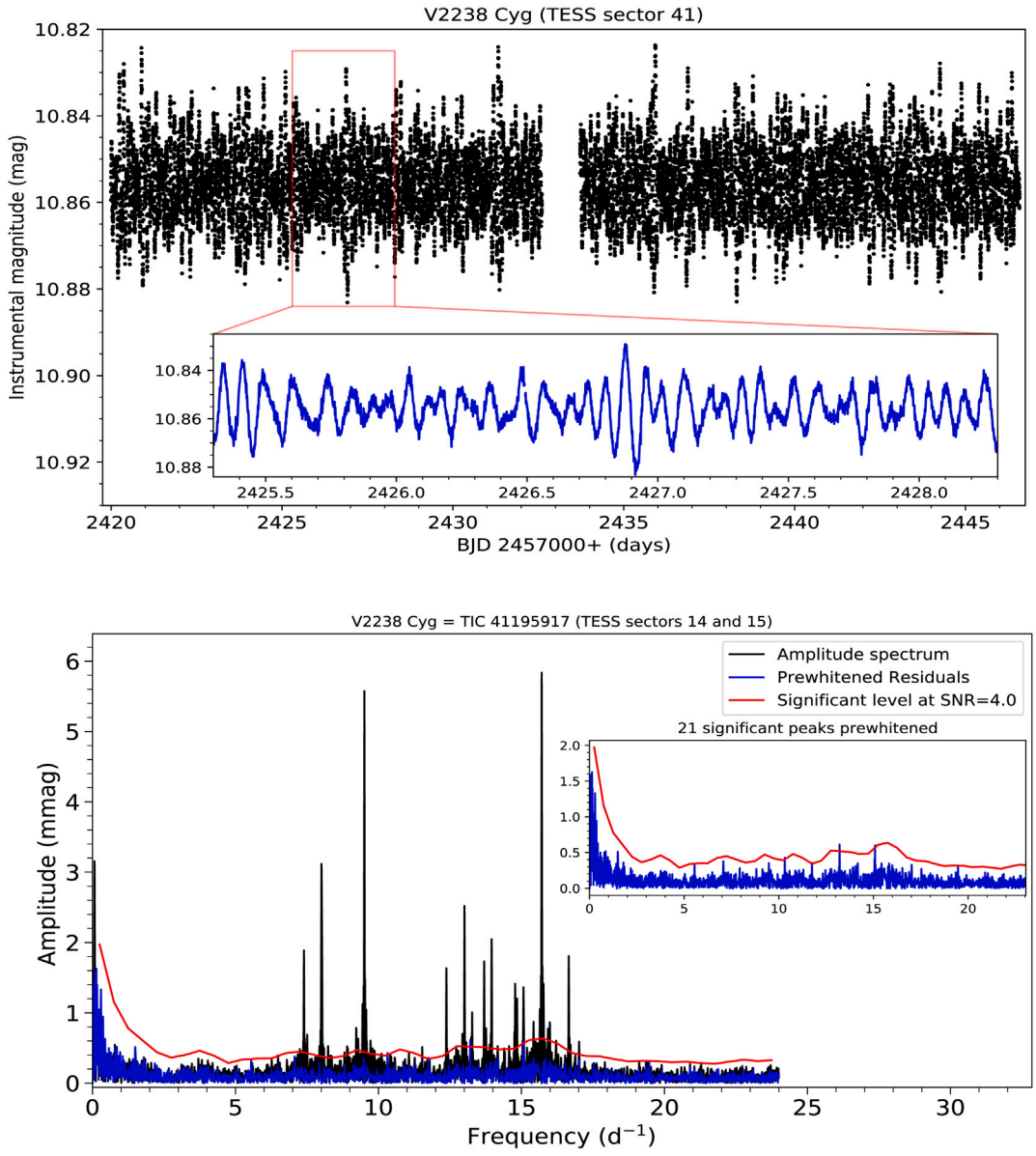

Fig. 2. *TESS* light curve of V2238 Cyg in Sector 41 (Top) and amplitude spectrum based on Sectors 14 and 15 with the inset showing the residuals (Bottom).

2 through 26, which resulted in five pulsation frequencies with millimag amplitudes at 19.76, 17.36, 16.69, 18.62 and 19.87 d^{-1} (Breger et al., 1993). This is one of the highest cited works in the δ Sct field. In addition, BU Cnc and BN Cnc were observed during the 1992 STEPHI IV campaign (lasting 3 weeks), where five and six frequency peaks were detected, respectively (Perez Hernandez et al., 1995). Reanalyzing the published photoelectric photometry using statistical weights significantly reduced noise levels, enabling the detection of seven frequencies in BU Cnc and eight in BN Cnc, including three previously unknown frequencies in BN Cnc (Arentoft et al., 1998). Table 5 lists the main stellar parameters for the four Praesepe members adopted from the *TESS* Input Catalog (TIC v8.2, Paegert et al., 2021).

Among the four stars, BN Cnc has *TESS* light curves available to public in sector 46 at MAST, HD 73712 has *TESS* light curves in sectors 44 and 46 at 2-min cadence. There are no *TESS* light curve data available for BU Cnc and BV Cnc by the time of this writing. However, *Kepler* K2 observed the Praesepe cluster area during 2015.04.27–2018.07.02 in Campaigns c05, c16 and c18. There are K2 data available for all the four stars. A total of 9450 data points were collected on actual 208 observing days over a time span of 1162.75 days. The K2 data provide a theoretical and efficient spectral resolution, of up to 0.00086 d^{-1} and 0.0048 d^{-1}, respectively. The superior frequency resolution and lower main alias level (at 0.000976 d^{-1}) of the K2 data compared to *TESS* data ensure that closely spaced frequencies can be better resolved. We analyzed K2 data for stars BU Cnc, BN Cnc, and BV Cnc, while analyzed both K2 and the two 2-min cadence *TESS* sectors data for HD 73712.

With *Kepler* K2 data, we resolved 26, 17, and 26 pulsation frequencies for BU Cnc, BN Cnc, and BV Cnc, respectively. Fig. 5 shows the periodogram for BU Cnc, where the low frequency region is very clean pure white noise showing lone-term stability of *Kepler* K2 photometry. The resolved significant pulsational frequencies are given in Table 6. For BN Cnc and BV Cnc, see Tables 7 and 8 for their frequency solution, Figs. 6 and 7 for their amplitude spectra, respectively. Our analysis successfully recovers six previously reported frequencies for BN Cnc (Arentoft et al., 1998) even when these frequencies exceed the Nyquist frequency of approximately 24.5 d^{-1}. Additionally, a new group of frequencies near 21 d^{-1} is revealed.

HD 73712 is a spectroscopic binary system with the primary component being a pulsating star of δ Sct type. We first applied frequency analyses to the K2 data and resolved 30 significant pulsational frequencies reported in Table 9. The *TESS* data which involved lower frequency

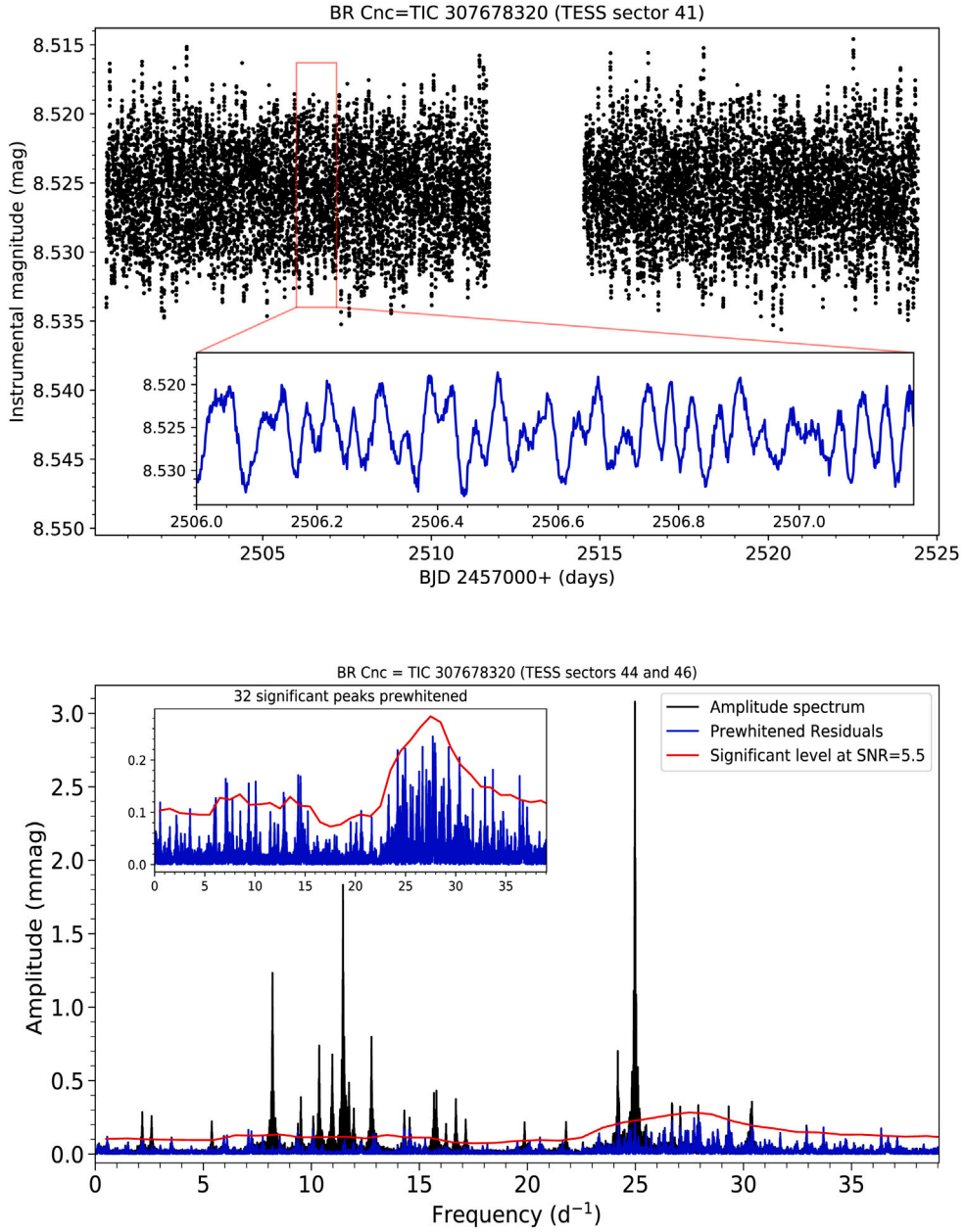

Fig. 3. *TESS* light curves in Sector 44 (upper) and amplitude spectrum of BR Cnc based on the two 2-min cadence Sectors 44 and 46.

resolution and less data coverage are also analyzed for comparison. We remark those frequencies detected in both sets of data in the *TESS* results in Table 10. Frequency contents within the frequency resolution of 0.0128 d^{-1} are considered common terms. The frequency patterns clearly show that HD 73712 is a hybrid δ Sct–γ Dor pulsator. Fig. 8 shows the periodograms based on the two sources of data and demo light curves from *TESS* sector 46.

4.3. NGC 2682: EX Cnc

EX Cnc (=TIC 437039231, B9V, $V = 10\overset{m}{.}92$, $B = 11\overset{m}{.}17$) is one of the members of the renowned solar-age Galactic open cluster NGC 2682 (also known as Messier 67, i.e. M67), it is a known δ Sct star observed by the author (Zhou, 2002, 2001). EX Cnc is also an oscillating blue straggler (assigned S1284) in M67 with five pulsation frequencies (Zhang et al., 2005). An earlier multisite campaign on the open cluster M67 in a time-baseline of 43 days revealed 26 pulsational frequencies for EX Cnc (Bruntt et al., 2007). However, the most recent simultaneous multi-color observations (in V, R, and I) aiming for mode identification led to just a single frequency solution of f_1 = 20.61 d^{-1} (Yakut et al., 2009).

TESS observed EX Cnc in four sectors 42, 44, 45, and 46 at 2-min cadence. Results of an attentive pulsational frequency analysis are presented in Table 11 and Fig. 9. There are multiple closely spaced terms distributed in three groups around 0.5, 5, and 20 d^{-1}, respectively. We first unveiled the two groups of lower-frequency pulsational contents which strongly suggest that EX Cnc is pulsating in hybrid δ Sct-γ Dor modes. We now validate the reality of both the aforementioned pulsation frequency f_1 = 20.61 d^{-1} and the term at ~19.6 d^{-1} that was suspected being daily alias in Yakut et al. (2009). Fortunately these authors "cannot exclude that 19.6 c/d is the correct frequency value". We compared our current frequency solution with literature values and adopted their labeling scheme. Besides three frequencies (f_{17}, f_{18}, and f_{19}), the rest 23 frequencies in the table 3 of Bruntt et al. (2007) are confirmed within an error bar given by the frequency resolution of the analyzed data. Concerning the long-term stability of *TESS* data, these

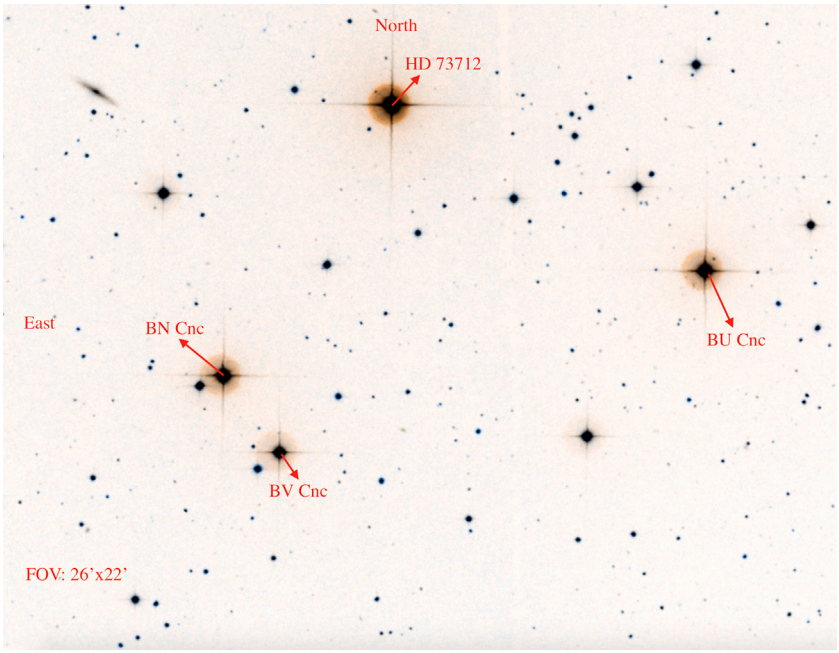

Fig. 4. Finding chart for BU Cnc, BV Cnc, BN Cnc and HD 73712 in the stellar cluster NGC 2632. The farthest separation between these stars is ~13 arcminutes, and the shortest separation is 2.5 arcminutes.

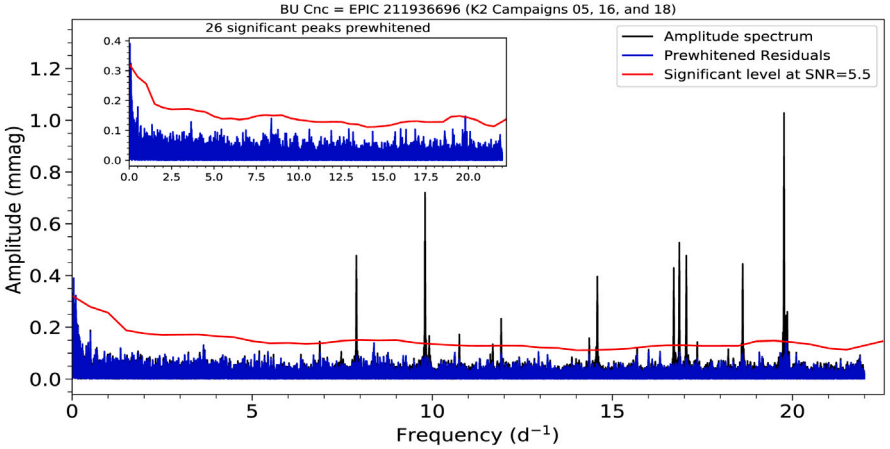

Fig. 5. Amplitude spectrum of BU Cnc based on *Kepler* K2 light curves on Campaigns c05, c16 and c18.

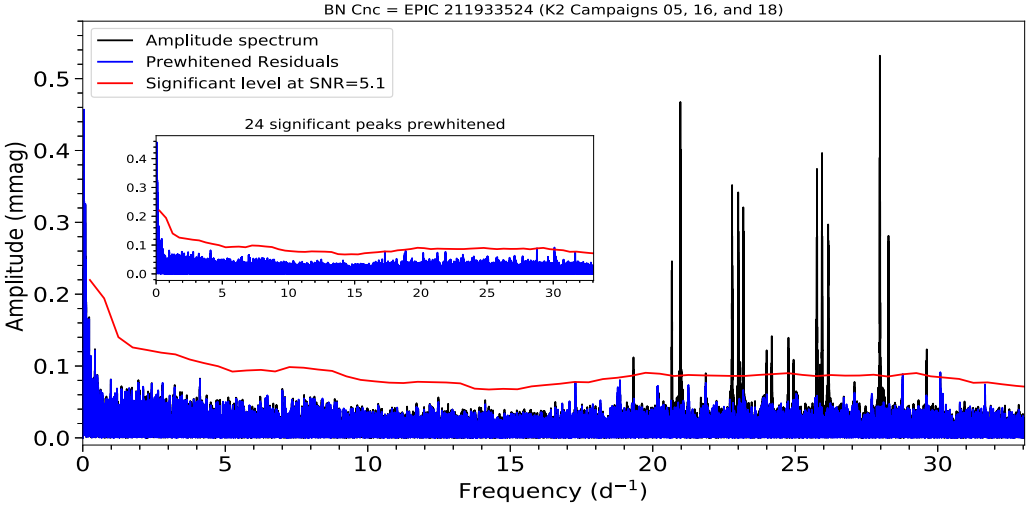

Fig. 6. Amplitude spectrum of BN Cnc based on *Kepler* K2 light curves on Campaigns c05, c16 and c18.

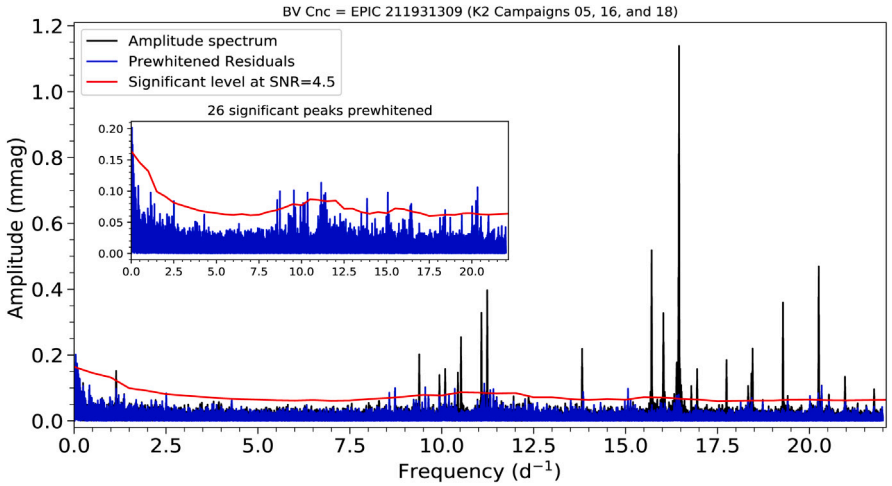

Fig. 7. Amplitude spectrum of BV Cnc based on *Kepler* K2 light curves on Campaigns c05, c16 and c18.

Table 6
Frequency solution of BU Cnc based on *Kepler* K2 mission campaigns 05, 16 and 18. The digits in parentheses represent the errors in the last two or three decimal places. The amplitude units are milli-magnitudes (mmag), with typical uncertainties of 0.0229 mmag. The previously detected frequencies are labeled by asterisks.

Frequency (d^{-1})	μHz	Amplitude	Phase (0-1)	SNR
f_0 = 19.767731(09)	∗228.79	1.199	0.4243(30)	46.3
f_1 = 9.799938(21)	∗113.43	0.885	0.1450(71)	36.0
f_2 = 7.893159(22)	91.36	0.613	0.0079(75)	22.3
f_3 = 18.619838(19)	∗215.51	0.579	0.1462(36)	24.8
f_4 = 16.706031(19)	∗193.36	0.566	0.0716(63)	23.8
f_5 = 16.859086(19)	∗195.13	0.514	0.3030(64)	21.6
f_6 = 17.054589(22)	197.39	0.485	0.6364(86)	20.3
f_7 = 14.584224(23)	168.80	0.480	0.7939(76)	23.6
f_8 = 11.913144(43)	137.88	0.254	0.0498(107)	10.8
f_9 = 19.858675(51)	∗229.85	0.211	0.1498(209)	8.2
f_{10} = 16.849761(65)	195.02	0.208	0.4233(216)	8.7
f_{11} = 19.828865(70)	229.50	0.201	0.4718(234)	7.8
f_{12} = 9.915434(62)	114.76	0.174	0.1073(101)	7.1
f_{13} = 10.752580(74)	124.45	0.168	0.1275(247)	7.2
f_{14} = 14.357945(54)	166.18	0.156	0.5617(181)	7.6
f_{15} = 6.874254(89)	79.56	0.154	0.0110(299)	6.1
f_{16} = 17.359629(52)	∗200.92	0.148	0.8552(175)	6.3
f_{17} = 16.874621(89)	195.31	0.131	0.7618(298)	5.5
f_{18} = 11.681082(84)	135.20	0.129	0.7620(283)	5.5
f_{19} = 18.219348(83)	210.87	0.122	0.0215(279)	5.2
Dependent frequencies within the effective frequency resolution 0.0048 d^{-1}				
$f_{20} = f_0 - 0.001145$	228.78	1.017	0.5451(36)	39.3
$f_{21} = f_1 - 0.002163$	113.40	0.602	0.6514(59)	24.5
$f_{22} = f_2 - 0.002186$	91.33	0.399	0.5958(60)	14.5
$f_{23} = f_3 - 0.00316$	215.47	0.362	0.9842(91)	15.5
$f_{24} = f_4 - 0.002141$	193.33	0.359	0.5248(173)	15.1
$f_{25} = f_6 - 0.001249$	197.38	0.422	0.0133(143)	17.7
$f_{26} = f_7 - 0.002183$	168.77	0.340	0.3531(100)	16.7
Theoretical frequency resolution: 0.000862 d^{-1} = 0.01 μHz				
Zeropoint: 0.00002268 mag				
Residuals: 0.00151853 mag				

Table 7
Frequency solution of BN Cnc based on *Kepler* K2 mission campaigns 05, 16 and 18. The digits in parentheses represent the error in the last two or three decimal places. The amplitude units are milli-magnitudes (mmag), with typical uncertainties of 0.019 mmag. Known frequencies are labeled by asterisks.

Frequency (d^{-1})	μHz	Amplitude	Phase (0-1)	SNR
f_0 = 20.971987(17)	242.73	0.486	0.8595(56)	28.8
f_1 = 27.969884(24)	∗323.73	0.341	0.4660(79)	19.8
f_2 = 25.940455(24)	∗300.24	0.333	0.5485(81)	19.7
f_3 = 22.783984(25)	∗263.70	0.321	0.8160(84)	19.0
f_4 = 23.176901(28)	268.25	0.289	0.0675(94)	17.1
f_5 = 23.187222(29)	268.37	0.281	0.5363(96)	16.6
f_6 = 24.176865(39)	∗279.82	0.205	0.5790(131)	11.8
f_7 = 22.998186(40)	266.18	0.203	0.0154(133)	12.0
f_8 = 23.002698(40)	∗266.23	0.202	0.5970(134)	11.9
f_9 = 20.982365(40)	242.85	0.202	0.1331(133)	12.0
f_{10} = 26.154517(42)	302.71	0.192	0.2260(141)	11.2
f_{11} = 19.323674(49)	223.65	0.165	0.4818(163)	9.8
f_{12} = 20.670855(53)	239.25	0.153	0.5178(176)	9.1
f_{13} = 28.271959(60)	∗327.22	0.134	0.9665(202)	8.0
f_{14} = 23.997385(67)	277.75	0.120	0.1232(224)	7.0
f_{15} = 23.169194(70)	268.16	0.115	0.6267(236)	6.8
f_{16} = 23.068174(81)	266.99	0.099	0.7431(272)	5.9
Dependent frequencies within the effective frequency resolution 0.0048 d^{-1}=0.056 μHz				
$f_{17} = f_0 - 0.003256$	242.69	0.467	0.0579(58)	27.7
$f_{18} = f_3 - 0.003226$	263.67	0.308	0.9685(88)	18.2
$f_{19} = f_6 + 0.003265$	268.41	0.223	0.2777(121)	13.2
$f_{20} = f_{12} + 0.00263$	239.28	0.137	0.3091(196)	8.1
$f_{21} = f_9 + 0.004163$	242.90	0.134	0.8729(201)	8.0
$f_{22} = f_6 - 0.003165$	279.79	0.135	0.5395(201)	7.7
$f_{23} = f_{11} + 0.004178$	223.70	0.130	0.1769(207)	7.7
Theoretical frequency resolution: 0.000861 d^{-1} = 0.01 μHz				
Zeropoint: −0.00000225 mag				
Residuals: 0.00111803 mag				

low frequencies are significant and they are interesting for exploring the star's pulsational prosperities.

4.4. TESS revisiting five field δ Sct stars

In this section, five field δ Sct stars previously observed by the author were reanalyzed using *TESS* data. The results are inspirational and have improved our knowledge on these stars' light variations largely. Below are separate summaries for each star.

4.4.1. AD Ari

AD Ari (= HD 14147 = TIC 246938869, F0, $V = 7\overset{m}{.}43$) might have been misclassified as a δ Sct stars. It was included in the δ Sct stars catalog by Rodríguez et al. (2000). Zhou (2002) observed the star on four nights with a result of 991 photometric measurements through two photoelectric 3-channel and 4-channel photometers. Due to the actual longer periodic light variations, the author only saw a portion of the periodic light variation at different phases each night and was unable to give an overall and accurate judgment on the star's variability.

With data from STEREO TRansiting Exoplanet and Stellar Survey, Sangaralingam and Stevens (2011) showed full periodic light curves with two distinct amplitudes and suspected that this star could be a binary system rather than a δ Sct star. Ziaali et al. (2019) derived a period–luminosity pair values of $\log P = -0.57, M_V = 2.26$ using *Gaia*

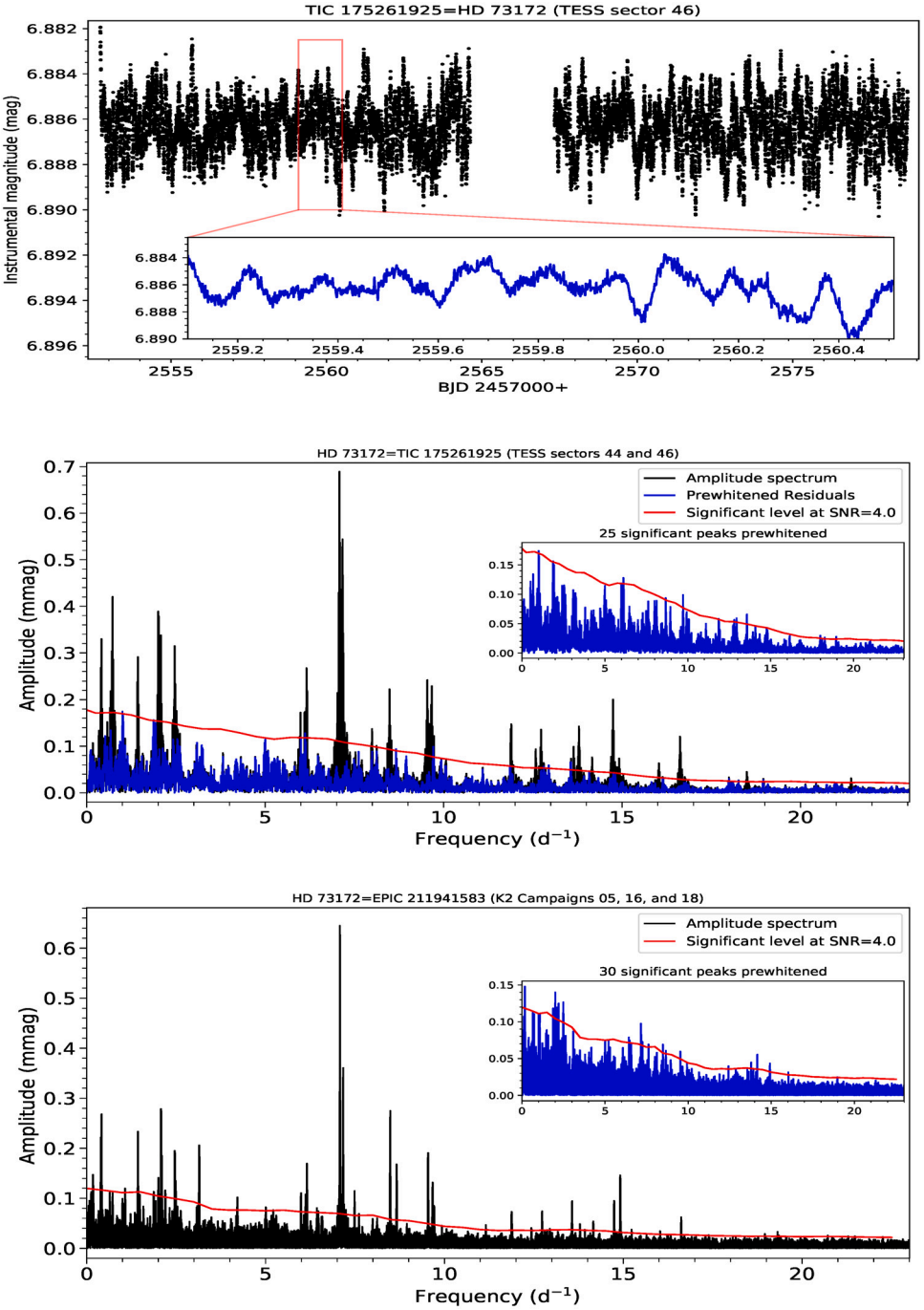

Fig. 8. *TESS* light curves in Sector 46 (upper) and amplitude spectra of HD 73172 based on two *TESS* sectors (middle) and *Kepler* K2 light curves in three campaigns (bottom).

DR2 parallaxes. They quoted the star as being an ellipsoid variable following Handler and Shobbrook (2002). There were no updates on the star's variability until *TESS*.

AD Ari was observed in two *TESS* sectors 42 and 43 in 2-min cadence. Uninterrupted monitors during four successive orbits, *TESS* collected perfect phase-coverage light curves which show distinct binary nature. The QLP team paid a close attention to the light curves' fitting for validating a possible transiting exoplanet. A Fourier analysis yielded three significant frequencies: $f_1 = 3.7060408\,\mathrm{d}^{-1}$ ($P_1 = 0.26983$ days), $f_2 = 1.8525275\,\mathrm{d}^{-1} = 0.5 f_1$ ($P_2 = 0.539803$ days), $f_3 = 5.5585683\,\mathrm{d}^{-1} = f_1 + f_2$. As the folded light curves shown now in Fig. 10, it is ultimately a rotating ellipsoidal binary variable, rather than a common contact eclipsing binary system, though having a rounded bottom during the primary eclipse and a deeper secondary eclipse.

4.4.2. ι Boo

ι Boo is a bright δ Sct star (=21 Boo = HR 5350 = HD 125161 = TIC 310381204, $V = 4\overset{\mathrm{m}}{.}75$, A7V). Earlier photoelectric photometry studies only revealed a single significant frequency content of $37.750 \pm 0.001\,\mathrm{d}^{-1}$ by Kiss et al. (1999a) and $37.6804\,\mathrm{d}^{-1}$ by Zhou (1999). Liakos and Niarchos (2017) listed the star as a suspected pulsator in an eclipsing binary system and adopted a dominant frequency of $37.750 \pm 0.001\ \mathrm{d}^{-1}$ according to the result of 1995–1998 photoelectric observations by Kiss et al. (1999b) and The Washington Double Star Catalog (Mason et al., 2001). This star is too bright to be a suitable target for telescopes sized over 50 cm with CCD photometry due to saturation issues concerning a reasonable CCD exposure time and restricted readout rates. However, *TESS* observed the star in four sectors 22, 23, 49, and 50 at 2-min cadence. The *TESS* stacked 2-min

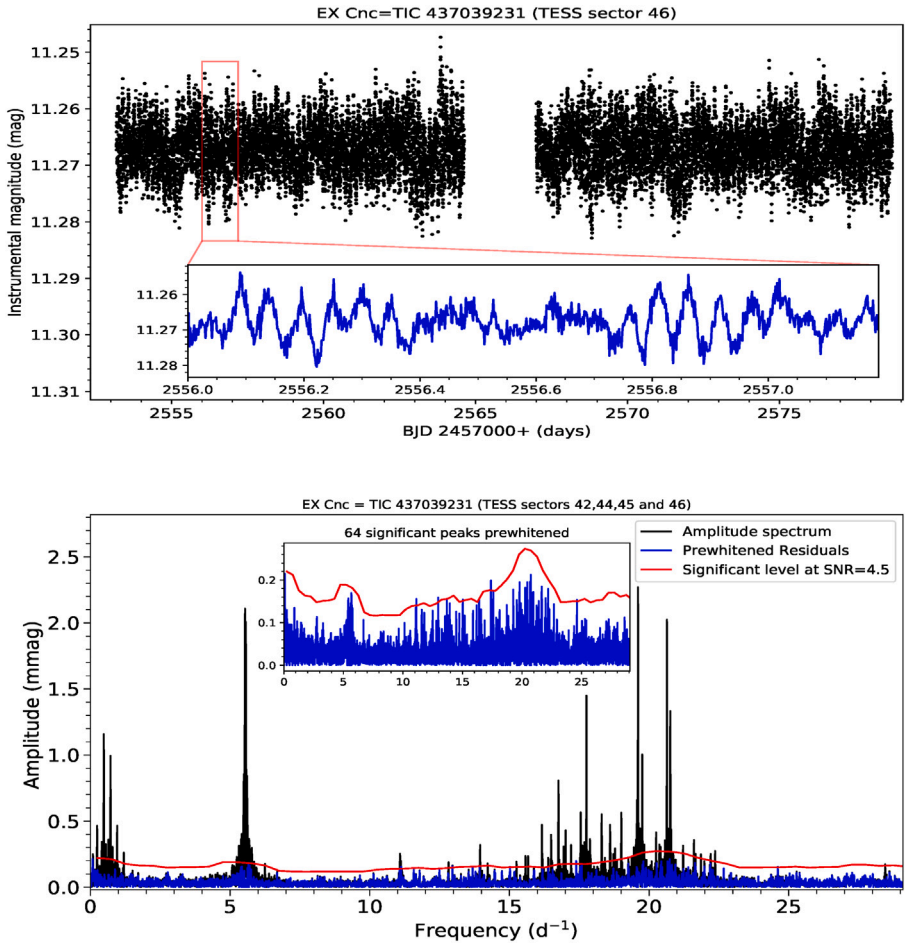

Fig. 9. *TESS* light curves in sector 46 (upper) and amplitude spectrum of EX Cnc based on *TESS* light curves in sectors 42, 44, 45, and 46.

cadence observations are good for a pulsation analysis. For this star, SAP fluxes are lined up and look like little systematic variations, thus SAP fluxes are used without extra processing.

The current available *TESS* data for ι Boo spanned $T = 792.19$ days, starting from BJD 2458899.3216408 to 2459691.51163725 (i.e. between 2020.02.19 19:43 and 2022.04.22 00:16 UT). There are observing gaps between two orbits in a sector (nearly a day, e.g. 0.96665 days in Sector 23, 0.90692 days in Sector 50), and between two successive sectors. In our case, 1.6125 days between sectors 22 and 23, 0.956937 days between sectors 49 and 50. These gaps would produce aliases similar to the daily aliases of ground observations. As a composite effect, the spectral window reflects the aliasing structure: in the current case, there is an evident alias at $a_1 = 0.001384$ d^{-1}. Nyquist sampling theorem indicates that a frequency peak will be accompanied by the combination side peaks at $f \pm n * a_1$ (n are integers). In fact, a_1 is less than frequency resolution discussed below, so aliasing issues will be removed effectively.

As seen now in Fig. 11, it is clear that the previous one-component sine wave function fitting (Kiss et al., 1999a; Zhou, 1999) is not enough to account for the light variations. The former main frequency should be a daily aliased value of the true dominant frequency $f_0 = 36.752011$ d^{-1}. The star is a single pulsating star not involved in a binary system. We present the pulsation contents of 74 significant frequencies with SNR exceeding 5.1 in Table 12, resolved by taking into account of an effective spectral resolution of 0.00912 d^{-1} (reciprocal of $4 * 27.4$ days) although the analyzed data give a theoretical frequency resolution of $\Delta f = 1/T = 0.001262$ d^{-1}. However, the residuals are not white noise yet. The complicated pulsation spectrum deserves further studies.

By the way, the author's previous work (Zhou, 1999) fortunately used 'star minus sky' measurements instead of differential magnitudes, which had a larger scatter very likely caused by the comparison star HD 234118 (= SAO 29066 = TIC 310381154, K2), a spectroscopic binary in Simbad, which turns out to be a rotating ellipsoidal variable in terms of *TESS* data.

4.4.3. IT Dra

IT Dra (= SAO 16394 = HD 127411 = TIC 166177270) is a δ Sct star that was first discovered by our group (Liu et al., 1998, 2000). *TESS* observed IT Dra in seven sectors (15, 16, 22, 23, 48, 49 and 50) in 2-min cadence during the period from BJD 2458711.3629 to 2459691.51 (i.e. in 2019.08.15–2022.04.22 UT). The data coverage is $13.7 * 2 * 7 = 191.8$ days (23523.5 h) with 127968 photometric measurements. The two previously detected frequencies ($f_1 = 16.8493$, $f_2 = 23.0613$ d^{-1}) are dominant and confirmed in *TESS* data, along with multiple additional pulsation contents. Results of the well-resolved 71 independent pulsational frequencies together with those unresolvable dependent frequencies are presented in Table 13. A significant frequency is detected with a SNR over 5.4 and resolved by the most conservative effective spectral resolution of 0.0052 d^{-1} calculated as the reciprocal of actual time length with data (191.8 days). Fig. 12 shows the *TESS* light curves in sector 49 and the amplitude spectrum based on all seven sectors data.

4.4.4. CD-54 7154

CD-54 7154 (= TIC 173503902 = ASAS 171022-5415.1, $B = 10\overset{m}{.}65$, $V = 10\overset{m}{.}26$) is a known δ Sct star with the GCVS designation of V0952 Ara (Kazarovets et al., 2015). It was first discovered as a δ Sct variable

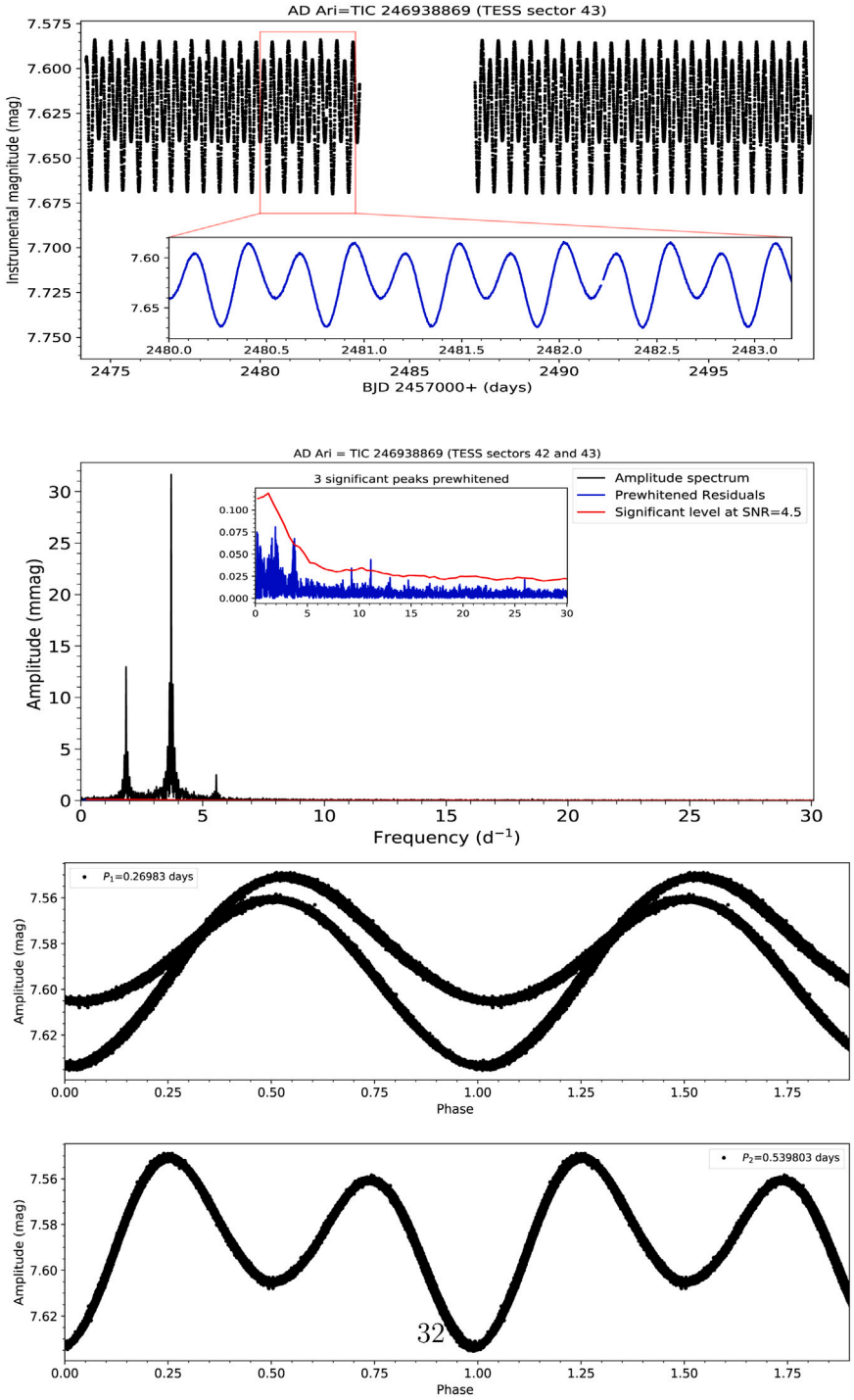

Fig. 10. *TESS* light curves (upper) and amplitude spectrum of AD Ari. The phase diagrams are folded using periods P_1 = 0.26983 and P_2 = 0.539803 days, respectively, with zero phase at BJD 2459447.88506, the first minimum in Sector 42.

star by ASAS (Pojmanski, 2002). The star's light curves obtained in *TESS* sectors 12 and 39 are notable for their conspicuous long-periodic light variations at a period of about 4.81 days, superimposed by shorter periodic variations (see Fig. 13). This at first glance resembles the dumbbell-shaped amplitude modulation.

Khruslov (2010) claimed multiperiodicity with nonradial pulsations and detected five pulsation frequencies: f_0 = 9.16355, f_1 = 9.36903, f_2 = 9.15744, f_3 = 9.15132, f_4 = 15.40360 d^{-1}. Frequencies f_0, f_1 and f_4 are confirmed in this work, while the others disappeared (see Table 14).

The visible amplitude modulation is caused by the beating between the two strongest close frequencies f_0 = 9.162285 and f_1 = 9.36902 d^{-1}. In stellar oscillation, the beating phenomenon refers to the temporary variation in the amplitude of an observed oscillation due to the interaction of two or more oscillation modes (pressure waves traveling through the star's interior) with slightly different frequencies. In this case, the beating frequency is $f_{\rm beat} = f_1 - f_0$ = 0.002408 d^{-1}, which corresponds to period $P_{\rm beat}$ = 4.8371 days. Additionally, the combination interaction of $f_{20} = f_0 + f_1 + 0.000117$ = 18.531305 d^{-1} is truly present in the frequency spectrum as well as a slight different term at f_{22} = 18.528015 d^{-1}.

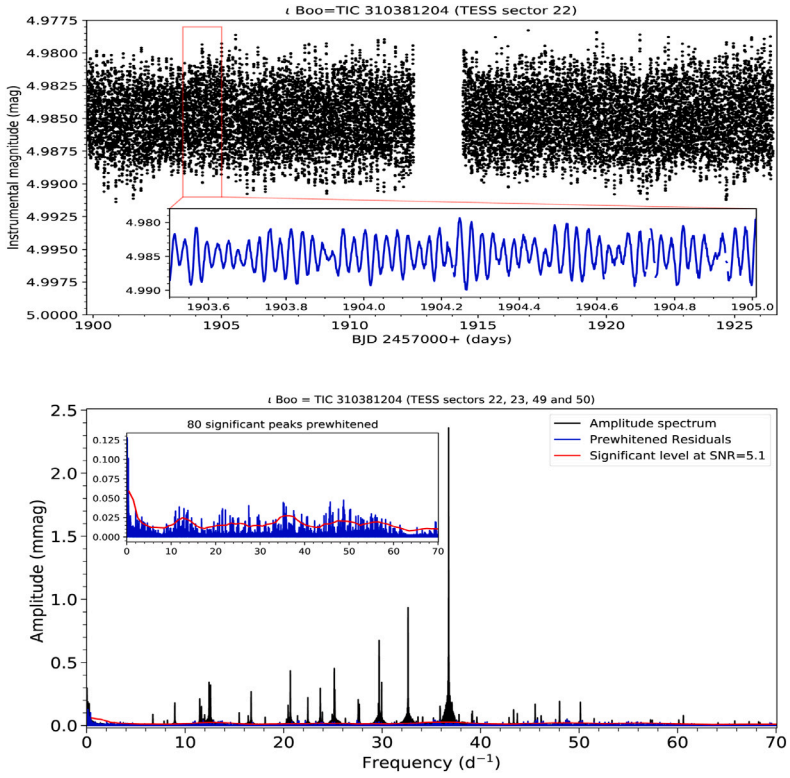

Fig. 11. *TESS* light curves in sector 22 and the amplitude spectrum of ι Boo based on the data in four sectors 22, 23, 49 and 50.

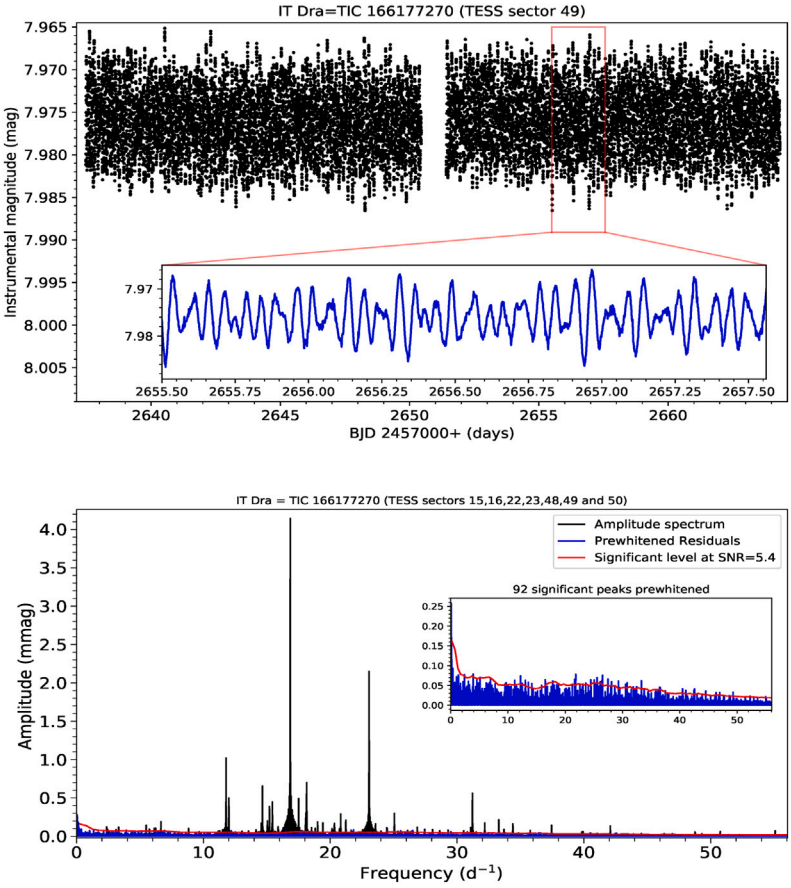

Fig. 12. Typical *TESS* light curves in sector 49 (upper) and the amplitude spectrum of IT Dra based on the data of all the available seven sectors 15, 16, 22, 23, 48, 49 and 50.

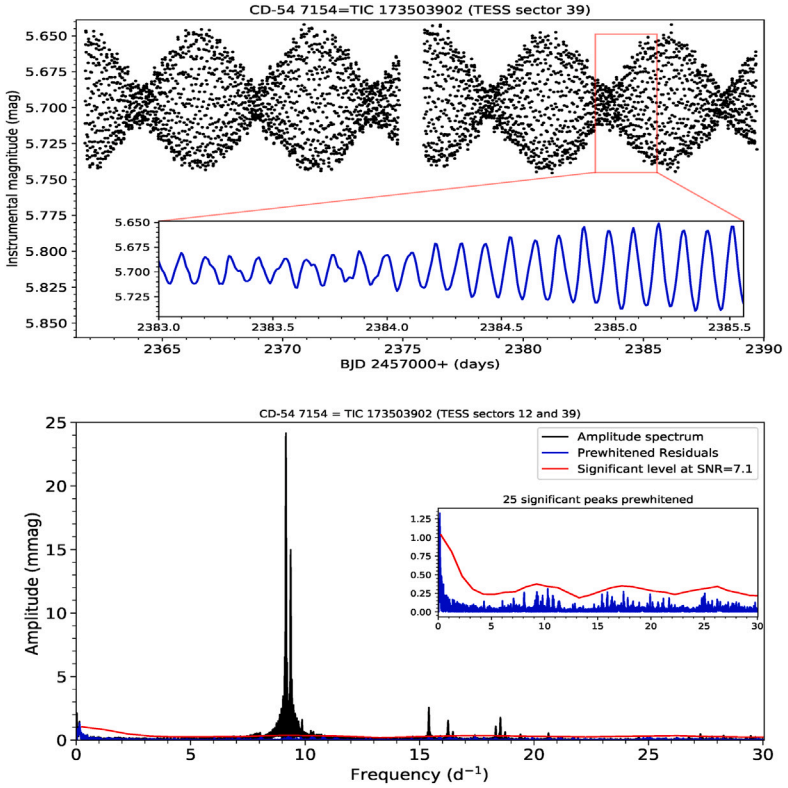

Fig. 13. *TESS* light curves in sector 39 and the amplitude spectrum of CD-54 7154(= TIC 173503902) based on the data in Sectors 12 and 39.

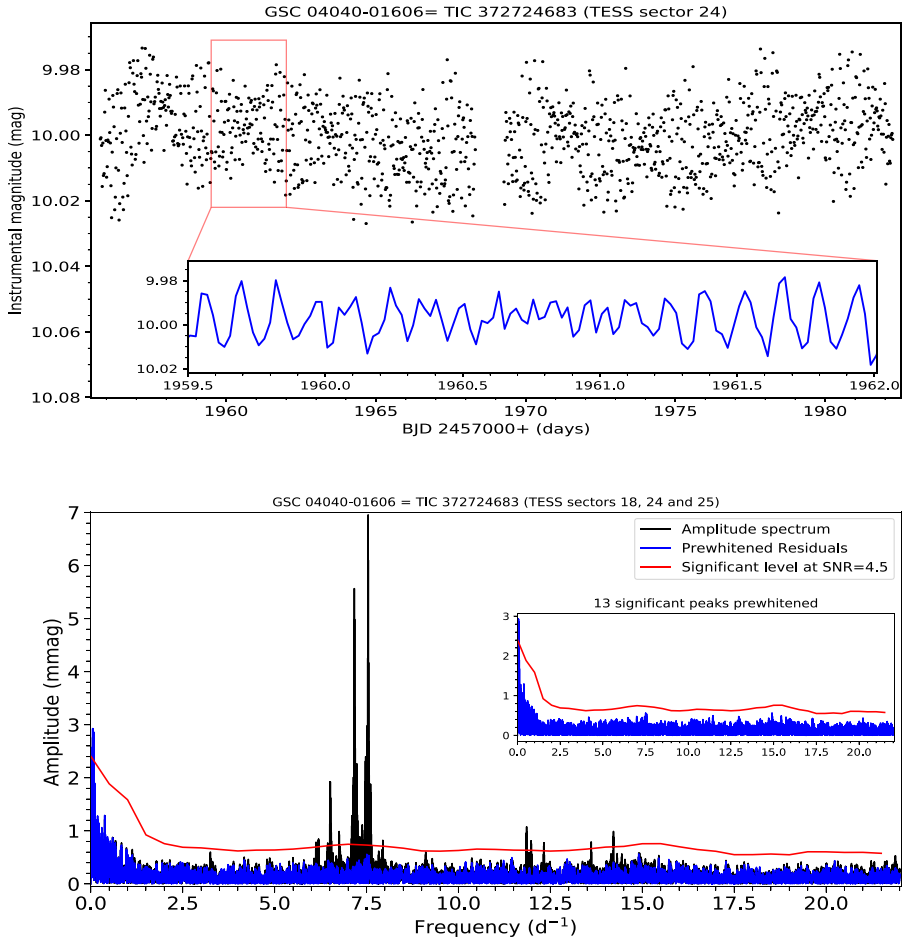

Fig. 14. *TESS* light curves in sector 24 and the amplitude spectrum of GSC 04040-01606(= TIC 372724683) based on the data in three sectors 18, 24, and 25.

Table 8
Frequency solution of BV Cnc based on *Kepler* K2 mission campaigns 05, 16 and 18. The digits in parentheses represent the error in the last two or three decimal places. The amplitude units are milli-magnitudes (mmag), with typical uncertainties of 0.0149 mmag. Known frequencies are labeled by asterisks.

Frequency (d^{-1})	μHz	Amplitude	Phase (0-1)	SNR
f_0 = 16.454138(06)	∗190.44	1.119	0.8445(21)	75.1
f_1 = 15.708030(16)	181.81	0.542	0.1481(52)	33.8
f_2 = 20.254236(19)	234.42	0.455	0.3553(62)	32.7
f_3 = 11.236416(31)	130.05	0.401	0.2922(102)	21.1
f_4 = 19.281025(29)	223.16	0.380	0.5151(96)	26.6
f_5 = 11.079418(45)	128.23	0.328	0.7031(151)	17.2
f_6 = 16.027988(63)	185.51	0.325	0.6541(212)	20.6
f_7 = 16.437150(13)	190.24	0.323	0.4650(44)	21.7
f_8 = 10.523808(22)	121.80	0.260	0.8337(73)	13.5
f_9 = 17.745867(30)	205.39	0.246	0.0926(101)	18.4
f_{10} = 13.818642(22)	159.94	0.234	0.6335(72)	16.6
f_{11} = 18.454742(27)	213.60	0.231	0.2104(91)	16.8
f_{12} = 9.387727(50)	108.65	0.215	0.2710(167)	12.2
f_{13} = 1.143246(45)	13.23	0.163	0.3746(150)	5.6
f_{14} = 10.093334(51)	116.82	0.158	0.2178(170)	9.2
f_{15} = 16.946492(33)	196.14	0.157	0.5382(110)	11.0
f_{16} = 16.388637(43)	189.68	0.141	0.4884(145)	9.5
f_{17} = 9.936352(73)	115.00	0.139	0.5719(244)	8.1
f_{18} = 18.421911(52)	213.22	0.138	0.9745(175)	10.1
f_{19} = 20.967817(51)	242.68	0.135	0.2245(171)	9.8
f_{20} = 16.037943(29)	185.62	0.126	0.3591(99)	8.0
f_{21} = 16.016966(56)	185.38	0.122	0.0645(188)	7.7
f_{22} = 18.333466(58)	212.19	0.112	0.3234(194)	8.1
f_{23} = 16.787254(50)	194.30	0.112	0.5194(168)	7.8
f_{24} = 21.760402(63)	251.86	0.097	0.0721(211)	7.0
Dependent frequencies within the effective frequency resolution 0.0048 d^{-1}				
$f_{25} = f_9$ + 0.000129	205.39	0.240	0.3487	18.0
f_{26} = $2f_0 - 2f_3$ − 0.002208	120.81	0.141	0.3537	7.3
Theoretical frequency resolution: 0.000861 d^{-1} = 0.01 μHz				
Zeropoint: −0.00000219 mag				
Residuals: 0.00099412 mag				

Table 9
Frequency solution of HD 73712 based on *Kepler* K2 mission campaigns 05, 16 and 18. The digits in parentheses represent the error in the last two or three decimal places. The amplitude units are milli-magnitudes (mmag), with typical uncertainties of 0.012 mmag. Known frequencies are labeled by asterisks.

Frequency (d^{-1})	μHz	Amplitude	Phase (0-1)	SNR
f_0 = 7.082444(20)	∗81.97	0.473	0.5895(67)	27.1
f_1 = 7.169653(21)	82.98	0.359	0.9749(70)	20.6
f_2 = 7.076171(22)	81.90	0.356	0.2096(74)	20.4
f_3 = 2.073726(24)	24.00	0.285	0.6395(80)	10.9
f_4 = 8.485967(05)	98.22	0.274	0.2331(17)	19.1
f_5 = 0.415086(06)	4.80	0.259	0.8646(19)	9.0
f_6 = 2.458471(31)	28.45	0.253	0.2978(103)	10.2
f_7 = 1.430804(92)	16.56	0.239	0.4499(309)	8.5
f_8 = 3.142627(16)	36.37	0.020	0.6493(54)	7.5
$f_9 = f_8$ + 0.00607	36.44	0.019	0.3568(45)	7.1
f_{10} = 0.394456(62)	4.57	0.203	0.5296(206)	7.0
f_{11} = 9.544075(39)	110.46	0.186	0.3896(132)	14.9
f_{12} = 2.093481(77)	24.23	0.183	0.1269(258)	7.0
f_{13} = 8.667229(74)	100.32	0.174	0.1555(250)	12.2
f_{14} = 6.154719(33)	71.24	0.159	0.0980(110)	8.7
f_{15} = 14.912859(12)	172.60	0.146	0.2689(41)	18.5
f_{16} = 9.671240(51)	111.94	0.140	0.3936(173)	11.2
f_{17} = 5.993164(23)	69.37	0.114	0.8954(76)	6.3
f_{18} = 7.088776(94)	82.05	0.111	0.2714(315)	6.4
f_{19} = 7.487203(98)	86.66	0.108	0.0619(329)	6.6
f_{20} = 6.118509(41)	70.82	0.108	0.0237(137)	5.9
f_{21} = 4.212949(36)	48.76	0.103	0.8947(121)	5.4
f_{22} = 13.570806(56)	157.07	0.093	0.5868(188)	10.0
f_{23} = 8.474514(67)	98.08	0.091	0.0592(226)	6.3
f_{24} = 9.713114(31)	112.42	0.089	0.0061(105)	7.1
f_{25} = 12.731512(65)	147.36	0.075	0.5353(217)	8.5
f_{26} = 16.617048(63)	192.33	0.062	0.0197(212)	8.4
f_{27} = 14.741815(50)	170.62	0.061	0.3857(168)	9.1
$f_{28} = f_{27}$ + 0.006542	170.70	0.059	0.8119(178)	7.0
f_{29} = 11.900878(53)	137.74	0.050	0.2468(177)	6.7
Dependent frequencies within the effective frequency resolution 0.0048 d^{-1} not available				
Theoretical frequency resolution: 0.000861 d^{-1}				
Zeropoint: 0.000007297 mag				
Residuals: 0.000806758 mag				

4.4.5. GSC 04040-01606

GSC 04040-01606 (= UCAC4 771-012013 = TIC 372724683 = *Gaia* DR3 5121436900712608 00, $B = 14\overset{m}{.}1$, $V = 14\overset{m}{.}01$) is a known δ Sct star whose variability was first claimed by Handler and Meingast (2011) during a search for new β Cephei stars in the young open cluster NGC 637. The star lies north of NGC 637 at an angular separation of about 10 arcminutes. Due to the limited data, it was suspected to be a multiple-frequency pulsator in the above literature. No further research was found. *TESS* observed the star in sectors 18, 24, and 25 at the 30-min cadence. Light curves are available as HLSP-QLP products. Based on the three sector data, we detected 14 significant pulsation frequencies with SNR over 4.5 resolved at an effective frequency resolution of 0.0122 d^{-1} against the theoretic one of 0.004575 d^{-1}. The frequencies and amplitudes are listed in Table 15. The light curves are shown in Fig. 14.

TIC v8.2 cataloged surface gravity $\log g$ = 3.23709, mass of 1.18 $M_\odot$, luminosity 24.63 $L_\odot$, and effective temperature $T_{\rm eff} = 6180 \pm 122$, but Gaia DR2 gives $T_{\rm eff}$ = 4909.9 K with an upper limit of 5014.9 K. Spectroscopy and multi-color photometry are useful in the future studies regarding the star's relative simple pulsation spectrum and easy mode identification.

5. Conclusions

The uninterrupted high-precision photometry from *TESS* and *Kepler* K2 has allowed us to better understand the real nature of stars that exhibit low-amplitude light variations. In this work, the author has made use of the space data to reanalyze 13 known δ Sct stars. Four stars' pulsational amplitudes are under 1.2 milli-magnitudes. These stars would not have been well resolved for their pulsation content in the previous short-term ground observations and fewer daily-gapped data. The highlights of this work are as follows:

- AD Ari, previously misclassified as δ Sct due to fewer data, is now identified to be a rotating ellipsoidal binary variable.
- Analysis revealed prominent beatings in the δ Sct star CD-54 7154, caused by a pair of closely spaced pulsation frequencies.
- ι Boo exhibits complex pulsations with over 73 distinct frequencies, as we only picked up those with SNR exceeding 5.1, leaving a number of peaks in the residual spectrum (see Fig. 11). It is not in an eclipsing binary system, as previously suspected in the literature (Liakos and Niarchos, 2017).
- More than 71 individual frequencies and 19 dependent terms were resolved in IT Dra with SNR above 5.4 (see Fig. 12).
- EX Cnc emerges as an exceptional δ Sct star due to its hybrid δ Sct–γ Dor nature revealed by the three distinct frequency groups shown in Fig. 9. HD 73712 is identified to be another hybrid δ Sct–γ Dor pulsator.
- *Kepler* K2 data greatly increased the number of pulsation frequencies of the three δ Sct stars: BU Cnc and BV Cnc from six to 26, and BN Cnc from eight to 17.
- The four stars BR Cnc, BU Cnc, BV Cnc, EX Cnc are in contrast to BN Cnc, which displays a simple Fourier spectrum, implying an easy mode identification. BR Cnc, BU Cnc, BV Cnc, HD 73712 are good seismic targets for their membership of NGC 2632.
- The three stars EX Cnc, ι Boo, and IT Dra are challenging targets for asteroseismic modeling.
- With high-precision and long-term space-borne photometry, we are able to reveal the true nature of a star's variability and discern its pulsational contents more clearly. Multiple stars in the selected group exhibit rich and regular pulsation patterns in their

Table 10
Frequency solution of HD 73712 (=TIC 175261925) based on *TESS* sectors 44 and 46. The digits in parentheses represent the error in the last two or three decimal places. The amplitude units are milli-magnitudes (mmag), with typical uncertainties of 0.0054 mmag. Last column 'K2' shows common terms resolved in both K2 and *TESS* data regarding the effective frequency resolution of 0.0128 d^{-1}, assigned with identical labels.

Frequency (d^{-1})	Amplitude	Phase (0-1)	SNR	K2
f_0 = 7.079656(57)	0.672	0.6302(13)	24.9	Yes
f_1 = 7.166453(72)	0.527	0.1646(16)	19.5	Yes
f_a = 0.723091(89)	0.427	0.6381(20)	9.9	–
f_b = 2.002063(111)	0.342	0.0295(25)	9.0	–
f_5 = 0.411645(111)	0.341	0.2907(25)	8.0	Yes
f_6 = 2.460935(119)	0.319	0.4582(27)	8.4	Yes
f_7 = 1.434695(125)	0.291	0.3408(33)	7.0	Yes
f_3 = 2.078010(133)	0.285	0.1466(30)	7.5	Yes
f_c = 6.157444(156)	0.270	0.9532(35)	9.2	–
f_{11} = 9.541868(144)	0.263	0.1767(33)	13.8	Yes
f_{16} = 9.668234(169)	0.250	0.8659(38)	13.1	Yes
f_4 = 8.482500(192)	0.224	0.8136(43)	9.3	Yes
f_{29} = 11.895700(263)	0.144	0.3172(59)	9.9	Yes
f_{17} = 5.985360(315)	0.138	0.1271(71)	4.6	Yes
f_d = 13.788900(284)	0.134	0.3091(64)	11.1	–
f_{26} = 16.619800(2457)	0.121	0.4265(556)	17.2	Yes
f_{25} = 12.730170(186)	0.120	0.6025(104)	9.0	Yes
f_f = 12.577700(152)	0.080	0.0129(34)	6.7	–
f_g = 14.915990(592)	0.073	0.8387(134)	6.9	–
f_h = 16.031650(517)	0.064	0.4800(117)	6.8	–
f_i = 18.491500(490)	0.045	0.6159(111)	8.1	–
f_j = 27.713280(468)	0.043	0.4090(106)	7.6	–
Combination and dependent frequencies within the resolution limit of 0.0128 d^{-1}				
$f_k = 2f_1 + f_4 - 0.002049$	0.198	0.7001	18.3	
$f_l = f_0 + 2f_1 - 0.002038$	0.029	0.9813	10.8	
$f_m = 2f_0 + 0.000232$	0.078	0.1448	6.0	
Zeropoint: 6.88636843 mag				
Residuals: 0.00068237 mag				

Table 11
Frequency solution of EX Cnc based on *TESS* sectors 42, 44, 45 and 46. The digits in parentheses represent the error in the last two or three decimal places. The amplitude units are milli-magnitudes (mmag), with typical uncertainties of 0.0162 mmag. The previously detected frequencies are marked by asterisks, while the last column 'Δ' gives the differences between current and literature of Bruntt et al. (2007).

Frequency (d^{-1})	μHz	Amplitude	Phase (0-1)	SNR	Δ (μHz)
f_1 = 19.604583(49)	∗226.90	2.318	0.1510(11)	40.1	0.01
f_2 = 20.639830(58)	∗238.89	1.984	0.1029(13)	33.2	0.01
f_3 = 20.759821(88)	∗240.28	1.298	0.2854(20)	21.7	0.02
f_4 = 16.530810(562)	∗191.33	0.203	0.2583(127)	5.3	0.13
f_5 = 19.563735(182)	∗226.43	0.629	0.0257(41)	10.9	0.02
f_6 = 17.758755(76)	∗205.54	1.504	0.1290(17)	38.8	0.06
f_7 = 19.757764(116)	∗228.68	0.986	0.3452(26)	17.1	0.02
f_8 = 18.603164(236)	∗215.31	0.483	0.1459(53)	10.8	0.02
f_9 = 17.013275(250)	∗196.91	0.457	0.9073(57)	11.7	0.05
f_{10} = 16.493099(295)	∗190.89	0.387	0.8837(67)	11.7	0.03
f_{11} = 18.782580(317)	∗217.39	0.361	0.1744(72)	8.0	0.04
f_{12} = 18.302547(189)	∗211.84	0.605	0.8262(43)	14.5	0.02
f_{13} = 16.941118(462)	∗196.08	0.247	0.3166(104)	6.4	0.07
f_{14} = 16.756059(143)	∗193.94	0.797	0.0506(32)	20.7	0.01
f_{15} = 19.006540(193)	∗219.98	0.591	0.1925(44)	11.9	0.03
f_{16} = 20.369790(103)	∗235.76	1.112	0.7519(23)	18.3	0.58
f_{17} = 17.553237(197)	∗203.16	0.579	0.8720(45)	14.9	0.03
f_{18} = –	∗223.01	–	–	–	–
f_{19} = –	∗258.86	–	–	–	–
f_{20} = –	∗199.45	–	–	–	–
f_{21} = 20.254370(299)	∗234.43	0.382	0.1479(68)	6.3	0.04
f_{23} = 21.608110(309)	∗250.09	0.370	0.6546(70)	7.5	0.56
f_{24} = 22.204720(461)	∗257.00	0.2480	0.2937	5.6	0.14
f_{25} = 15.668230(527)	∗181.35	0.217	0.5016(119)	6.3	0.74
f_{26} = 12.823290(605)	∗148.42	0.189	0.5663(137)	5.9	0.12
f_{27} = 5.536208(47)	64.08	2.418	0.6912(11)	60.0	
f_{28} = 5.557908(50)	64.33	2.278	0.4349(11)	56.5	
f_{29} = 5.573865(81)	64.51	1.406	0.0742(18)	34.9	
f_{30} = 5.520251(106)	63.89	1.083	0.0472(24)	26.9	
f_{31} = 0.478052(94)	5.53	1.212	0.1337(21)	24.8	
f_{32} = 0.717397(106)	8.30	1.076	0.1275(24)	22.8	
f_{33} = 5.475574(135)	63.37	0.848	0.9242(30)	20.2	
f_{34} = 5.608968(171)	64.92	0.669	0.1231(39)	16.6	
f_{35} = 5.593650(247)	64.74	0.506	0.6575(56)	11.4	

(*continued on next page*)

Table 11 (*continued*).

Frequency (d^{-1})	μHz	Amplitude	Phase (0-1)	SNR	Δ (μHz)
f_{36} = 0.955465(228)	11.06	0.502	0.6866(51)	10.6	
f_{37} = 16.163760(235)	187.08	0.487	0.0405(53)	14.8	
f_{38} = 16.163760(258)	187.08	0.484	0.0415(58)	9.8	
f_{39} = 0.237430(259)	2.75	0.482	0.5553(59)	10.4	
f_{40} = 17.880080(308)	206.95	0.371	0.3512(70)	9.6	
f_{41} = 5.640800(342)	65.29	0.334	0.7625(77)	8.3	
f_{42} = 5.402200(340)	62.53	0.336	0.0815(77)	8.0	
f_{43} = 17.208950(348)	199.18	0.328	0.9715(79)	8.4	
f_{44} = 21.217449(354)	245.57	0.323	0.7481(80)	5.7	
f_{45} = 13.951290(356)	161.47	0.321	0.9703(80)	9.3	
f_{46} = 5.445705(373)	63.03	0.306	0.4527(84)	7.3	
f_{47} = 1.194708(418)	13.83	0.274	0.1501(94)	7.0	
f_{48} = 21.859160(463)	253.00	0.246	0.7795(105)	5.0	
f_{49} = 5.677930(472)	65.72	0.242	0.6556(107)	6.0	
f_{50} = 15.575570(489)	180.27	0.233	0.6221(111)	6.7	
f_{51} = 5.324946(518)	61.63	0.221	0.7568(117)	5.3	
f_{52} = 18.287926(543)	211.67	0.210	0.8207(123)	5.1	
f_{53} = 18.420590(583)	213.20	0.196	0.3977(132)	4.7	
f_{54} = 14.220298(629)	164.59	0.182	0.8162(142)	5.0	
f_{55} = 15.252830(594)	176.54	0.192	0.0392(134)	5.7	
f_{56} = 6.247450(674)	72.31	0.170	0.8763(152)	4.6	
f_{57} = 28.453980(686)	329.33	0.167	0.4791(155)	4.7	
Dependent frequencies within the effective frequency resolution 0.0128 d^{-1}					
$f_{58} = 3f_{27} - 2f_{29} - 0.003828$		0.6250	0.3211	14.9	
$f_{59} = 3f_{27} - 2f_{35} - 0.005106$		0.5060	0.6701	12.1	
$f_{60} = f_{27} + f_{29} + 0.008686$		0.2510	0.9152	8.0	
$f_{61} = f_{28} + 0.01058$		0.264	0.8526	6.5	
$f_{62} = f_{27} + f_{35} + 0.002053$		0.1960	0.0855	6.3	
$f_{63} = f_{8} + 0.01016$		0.255	0.9434	5.7	
$f_{64} = f_{27} + 3f_{29} + 0.005212$		0.2480	0.2937	5.6	
Theoretical frequency resolution: 0.012735 d^{-1} = 9 μHz Zeropoint: 11.2592026 mag Residuals: 0.00276131 mag					

Table 12
Frequency solution of ι Boo based on *TESS* data in sectors 22,23,49 and 50. The digits in parentheses represent the error in the last two or three decimal places. The amplitude units are milli-magnitudes (mmag), with typical uncertainties of 0.0019 mmag. The previously detected frequency is marked by asterisks.

Frequency (d^{-1})	μHz	Amplitude	Phase (0-1)	SNR
f_0 = *36.752011(01)	425.37	2.363	0.8038(01)	439.3
f_1 = 32.632110(01)	377.69	0.935	0.1384(03)	276.8
f_2 = 29.694026(02)	343.68	0.678	0.3058(05)	231.7
f_3 = 25.142709(03)	291.00	0.488	0.1928(06)	141.3
f_4 = 20.680305(03)	239.36	0.437	0.9876(07)	148.8
f_5 = 29.950102(04)	346.64	0.353	0.2790(09)	120.6
f_6 = 12.425427(04)	143.81	0.353	0.2141(09)	73.4
f_7 = 12.577021(04)	145.57	0.325	0.4000(10)	67.5
f_8 = 25.200827(04)	291.68	0.327	0.8082(09)	94.7
f_9 = 23.724616(05)	274.59	0.294	0.7578(10)	82.9
f_{10} = 22.456986(06)	259.92	0.222	0.3831(14)	73.3
f_{11} = 16.697468(05)	193.26	0.267	0.9036(12)	114.4
f_{12} = 11.482119(06)	132.89	0.209	0.6106(15)	49.7
f_{13} = 27.568840(07)	319.08	0.198	0.3496(16)	76.2
f_{14} = 48.018360(07)	555.77	0.190	0.0395(16)	47.4
f_{15} = 50.137099(07)	580.29	0.182	0.1640(17)	47.5
f_{16} = 8.950240(08)	103.59	0.179	0.1281(17)	78.7
f_{17} = 27.679861(08)	320.37	0.169	0.0955(18)	64.9
f_{18} = 45.536400(08)	527.04	0.167	0.6224(18)	50.7
f_{19} = 29.617119(08)	342.79	0.168	0.6383(18)	57.3
f_{20} = 20.450560(09)	236.70	0.158	0.1718(20)	53.7
f_{21} = 35.879740(09)	415.27	0.143	0.1803(22)	26.7
f_{22} = 11.656840(10)	134.92	0.140	0.3965(22)	33.5
f_{23} = 37.090820(10)	429.29	0.133	0.4618(23)	25.8
f_{24} = 43.350000(11)	501.74	0.124	0.8946(25)	49.1
f_{25} = 39.157760(12)	453.21	0.117	0.6053(26)	34.4
f_{26} = 35.896580(12)	415.47	0.114	0.3440(27)	21.3
f_{27} = 23.929040(13)	276.96	0.106	0.9423(29)	29.8
f_{28} = 36.767840(13)	425.55	0.101	0.3084(31)	18.8
f_{29} = 15.487619(14)	179.25	0.097	0.8693(32)	32.7
f_{30} = 43.722060(14)	506.04	0.097	0.1061(32)	38.3
f_{31} = 39.105500(15)	452.61	0.093	0.3423(33)	27.3
f_{32} = 25.129980(14)	290.86	0.093	0.1167(33)	27.0

(*continued on next page*)

Table 12 (*continued*).

Frequency (d^{-1})	μHz	Amplitude	Phase (0-1)	SNR
f_{33} = 11.979180(15)	138.65	0.089	0.8055(35)	21.1
f_{34} = 6.720160(15)	77.78	0.089	0.5227(35)	36.6
f_{35} = 21.410680(17)	247.81	0.080	0.9329(39)	26.9
f_{36} = 37.362980(17)	432.44	0.080	0.3232(39)	15.6
f_{37} = 16.402560(17)	189.84	0.079	0.8239(39)	33.8
f_{38} = 37.806800(17)	437.58	0.077	0.0211(40)	15.1
f_{39} = 34.115580(18)	394.86	0.077	0.6681(40)	15.6
f_{40} = 46.144740(18)	534.08	0.075	0.9266(41)	20.7
f_{41} = 25.151930(19)	291.11	0.070	0.0544(44)	20.3
f_{42} = 39.617700(21)	458.54	0.064	0.7103(48)	18.9
f_{43} = 18.125060(22)	209.78	0.063	0.3883(49)	25.1
f_{44} = 36.306945(22)	420.22	0.061	0.2825(50)	11.4
f_{45} = 42.887000(22)	496.38	0.060	0.3982(51)	24.7
f_{46} = 24.931001(23)	288.55	0.058	0.4495(53)	17.8
f_{47} = 33.643310(24)	389.39	0.057	0.1822(54)	15.3
f_{48} = 12.558130(24)	145.35	0.057	0.9624(54)	11.8
f_{49} = 33.089422(25)	382.98	0.055	0.2823(56)	14.8
f_{50} = 26.271100(26)	304.06	0.053	0.8588(58)	16.2
f_{51} = 60.587629(26)	701.25	0.052	0.5132(60)	20.4
f_{52} = 51.524101(27)	596.34	0.050	0.2279(62)	14.1
f_{53} = 20.299088(27)	234.94	0.049	0.1018(63)	16.8
f_{54} = 36.614240(28)	423.78	0.048	0.4593(64)	9.0
f_{55} = 57.254387(30)	662.67	0.045	0.3807(68)	12.8
f_{56} = 60.125610(31)	695.90	0.043	0.2850(72)	17.0
f_{57} = 45.771298(32)	529.76	0.043	0.5252(72)	12.9
f_{58} = 57.426300(32)	664.66	0.042	0.9215(73)	11.9
f_{59} = 12.593170(24)	145.75	0.042	0.9692(54)	8.8
f_{60} = 8.199867(32)	94.91	0.042	0.1179(74)	18.5
f_{61} = 53.340400(33)	617.37	0.041	0.0681(76)	12.4
f_{62} = 29.364901(34)	339.87	0.040	0.9418(77)	13.7
f_{63} = 36.414500(37)	421.46	0.036	0.9748(85)	6.7
f_{64} = 65.807070(38)	761.66	0.036	0.6490(86)	19.5
f_{65} = 25.117000(41)	290.71	0.033	0.1554(94)	9.5
f_{66} = 7.856200(43)	90.93	0.032	0.8680(98)	13.6
f_{67} = 36.780525(43)	425.70	0.032	0.5866(98)	5.9
f_{68} = 67.259730(43)	778.47	0.031	0.4437(98)	14.4
f_{69} = 68.228050(49)	789.68	0.028	0.9328(112)	13.5
f_{70} = 35.208497(49)	407.51	0.027	0.0616(113)	5.1
f_{71} = 64.107990(61)	741.99	0.022	0.8777(139)	13.4
f_{72} = 68.372790(66)	791.35	0.020	0.2937(151)	9.9
f_{73} = 31.468100(37)	364.21	0.019	0.5790(85)	6.0
Dependent frequencies within the effective frequency resolution 0.00912 d^{-1}				
$f_{74} = f_{41} - 0.001470$	291.09	0.059	0.3827(52)	17.1
$f_{75} = f_{51} - 0.000579$	701.24	0.049	0.3811(62)	19.5
$f_{76} = 2f_0$		0.0170	0.7743	11.2
$f_{77} = f_0 - 0.006131$	425.30	0.038	0.4325(82)	7.0
$f_{78} = f_{47} + 0.000672$	389.40	0.025	0.8057(124)	6.7
$f_{79} = 2f_3 + f_4 - 0.007377$	0.0210	0.8759	11.0	
$f_{80} = 3f_1 - 2f_3 - 0.003885$	0.0280	0.1879	6.9	
Theoretical frequency resolution: 0.001262 d^{-1}				
Zeropoint: 4.9513359 mag				
Residuals: 0.000375055316 mag				

Table 13
Frequency solution of IT Dra based on *TESS* sectors 15, 16, 22, 23, 48, 49 and 50. The digits in parentheses represent the error in the last two or three decimal places. The amplitude units are milli-magnitudes (mmag), with typical uncertainties of 0.0039 mmag. The previously detected frequencies are marked by asterisks.

Frequency (d^{-1})	μHz	Amplitude (mmag)	Phase (0-1)	SNR
f_0 = *16.850786(01)	195.03	4.124	0.6811(02)	419.5
f_1 = *23.062767(01)	266.93	2.089	0.3999(03)	219.4
f_2 = 11.785623(02)	136.41	1.014	0.2738(06)	103.8
f_3 = 18.141353(03)	209.97	0.699	0.4737(09)	63.4
f_4 = 14.656449(03)	169.63	0.655	0.2176(10)	83.7
f_5 = 31.213879(04)	361.27	0.572	0.7476(11)	65.6
f_6 = 17.507855(04)	202.64	0.515	0.3725(12)	48.3
f_7 = 12.004582(05)	138.94	0.489	0.5302(13)	49.6
f_8 = 15.442096(05)	178.73	0.464	0.9629(13)	58.8
f_9 = 15.208178(06)	176.02	0.381	0.2623(16)	48.3
f_{10} = 25.060636(07)	290.05	0.304	0.5506(21)	29.4
f_{11} = 20.825305(07)	241.03	0.294	0.3958(21)	31.7

(*continued on next page*)

Table 13 (*continued*).

Frequency (d^{-1})	μHz	Amplitude (mmag)	Phase (0-1)	SNR
f_{12} = 18.078680(08)	209.24	0.283	0.5877(22)	25.6
f_{13} = 0.036672(08)	0.42	0.266	0.0564(23)	9.0
f_{14} = 33.289025(10)	385.29	0.232	0.1260(27)	30.4
f_{15} = 32.187801(13)	372.54	0.172	0.6326(36)	22.6
f_{16} = 34.398346(13)	398.13	0.164	0.4014(38)	21.9
f_{17} = 37.454100(15)	433.50	0.146	0.0440(43)	22.5
f_{18} = 42.082750(16)	487.07	0.134	0.0220(46)	26.0
f_{19} = 55.084270(31)	637.55	0.072	0.6614(87)	20.5
f_{20} = 50.749873(36)	587.38	0.061	0.6373(102)	15.2
f_{21} = 48.768254(40)	564.45	0.056	0.5698(112)	12.9
f_{22} = 21.232822(12)	245.75	0.189	0.9484(33)	19.1
f_{23} = 14.564082(14)	168.57	0.160	0.7639(39)	20.4
f_{24} = 6.656792(11)	77.05	0.192	0.5780(32)	14.6
f_{25} = 8.834044(21)	102.25	0.106	0.8273(59)	11.1
f_{26} = 19.008615(13)	220.01	0.176	0.1575(35)	18.7
f_{27} = 19.425886(13)	224.84	0.165	0.0135(38)	17.5
f_{28} = 15.049642(11)	174.19	0.207	0.1489(30)	26.2
f_{29} = 23.574049(02)	272.85	1.3500	0.2389	136.8
f_{30} = 39.934970(37)	462.21	0.059	0.8579(105)	10.8
f_{31} = 20.331594(14)	235.32	0.154	0.4418(40)	16.6
f_{32} = 18.042950(17)	208.83	0.130	0.7385(48)	11.8
f_{33} = 18.535810(26)	214.53	0.086	0.8948(72)	8.5
f_{34} = 15.884880(22)	183.85	0.102	0.4798(61)	12.3
f_{35} = 18.820119(16)	217.83	0.134	0.1155(46)	13.3
f_{36} = 24.456255(27)	283.06	0.081	0.6745(77)	8.9
f_{37} = 24.495975(30)	283.52	0.073	0.8746(85)	8.1
f_{38} = 25.035300(31)	289.76	0.071	0.9912(87)	6.9
f_{39} =26.865194(21)	310.94	0.107	0.6335(58)	11.8
f_{40} = 14.144850(24)	163.71	0.094	0.6514(67)	11.7
f_{41} = 27.459350(43)	317.82	0.051	0.4261(122)	5.5
f_{42} = 28.073580(36)	324.93	0.062	0.4781(101)	6.8
f_{43} = 28.640780(37)	331.49	0.0600	0.7838	6.6
f_{44} = 30.525790(30)	353.31	0.073	0.6111(85)	9.2
f_{45} = 31.065240(45)	359.55	0.049	0.2825(127)	5.6
f_{46} = 31.070716(43)	359.61	0.051	0.3376(123)	5.8
f_{47} = 33.701670(25)	390.07	0.0890	0.4775	11.6
f_{48} = 35.770920(29)	414.02	0.077	0.6171(81)	10.5
f_{49} = 39.831920(41)	461.02	0.053	0.9772(117)	9.7
f_{50} = 40.536060(50)	469.17	0.044	0.9152(141)	8.0
f_{51} = 20.730160(21)	239.93	0.105	0.0970(60)	11.3
f_{52} = 20.136625(23)	233.06	0.094	0.3928(66)	10.1
f_{53} = 5.742250(25)	66.46	0.088	0.9376(71)	6.9
f_{54} = 20.209454(26)	233.91	0.085	0.2973(73)	9.2
f_{55} = 15.924470(27)	184.31	0.083	0.0440(75)	9.9
f_{56} = 16.512520(27)	191.12	0.083	0.9523(75)	8.4
f_{57} = 15.404060(32)	178.29	0.070	0.4152(89)	8.8
f_{58} = 17.577664(25)	203.45	0.087	0.0545(71)	8.2
f_{59} = 15.639730(38)	181.02	0.059	0.2401(106)	7.0
f_{60} = 15.735250(49)	182.12	0.045	0.5122(138)	5.4
f_{61} = 16.146690(42)	186.88	0.052	0.3339(120)	6.1
f_{62} = 5.492620(16)	63.57	0.141	0.9773(44)	10.9
f_{63} = 3.318598(18)	38.41	0.121	0.6376(52)	9.3
f_{64} = 2.370830(18)	27.44	0.121	0.6178(52)	8.6
f_{65} = 6.125770(21)	70.90	0.103	0.4185(60)	7.9
f_{66} = 6.235430(20)	72.17	0.108	0.0129(58)	8.3
f_{67} = 3.116365(25)	36.07	0.087	0.9967(71)	6.7
f_{68} = 2.439138(24)	28.23	0.090	0.3127(69)	6.4
$f_{69} = f_0 + 0.007436$ = 16.843350(17)	194.95	0.128	0.4374(49)	13.0
$f_{70} = f_1 - 0.008875$ = 23.053892(14)	266.83	0.155	0.8534(40)	16.2
$f_{71} = f_1 - 0.007126$ = 23.055640(16)	266.85	0.134	0.8558(47)	14.1
Dependent frequencies within the effective frequency resolution 0.00521 d^{-1}				
$f_0 + 0.002089$ = 16.852875(06)	195.06	0.364	0.3131(17)	37.1
$f_1 - 0.001716$ = 23.061051(03)	266.91	0.721	0.8505(09)	75.7
$2f_2 - 0.002803$		1.3500	0.2389	136.8
$f_5 + 0.001861$ = 31.215740(23)	361.29	0.096	0.8730(65)	11.0
$f_8 - 0.002704$ = 15.444800(30)	178.76	0.074	0.2602(84)	9.4
$f_{10} + 0.001864$ = 25.062500(36)	290.08	0.061	0.8381(102)	5.9
$f_{15} - 0.001975$ = 33.287050(19)	385.27	0.113	0.8489(55)	14.9
$f_{16} - 0.000409$ = 34.398755(21)	398.13	0.105	0.3820(59)	14.0

(*continued on next page*)

frequency spectra. Several stars are now updated with a couple of dozen frequencies, which is a significant improvement from the previous ground photometry results of a few.

Probing and using pulsation frequencies is an effective way to gain insights into stellar structure. Simple pulsation spectra facilitate identification of oscillation modes and their modeling. Complex pulsation

Table 13 (*continued*).

Frequency (d^{-1})	μHz	Amplitude (mmag)	Phase (0-1)	SNR
$f_{22} - 0.0005259 = 21.232296(18)$	245.74	0.121	0.4970(51)	12.2
$f_{28} - 0.0034679 = 15.053110(19)$	174.23	0.118	0.3219(53)	14.9
$f_{31} - 0.004901 = 20.336495(25)$	235.38	0.089	0.4073(70)	9.6
$f_{31} - 0.0006239 = 20.330970(28)$	235.31	0.078	0.8029(80)	8.4
$f_{32} - 0.000885 = 18.043835(14)$	208.84	0.162	0.4536(38)	14.7
$f_{33} - 0.0004640 = 18.535346(21)$	214.53	0.106	0.4295(59)	10.4
$f_{35} + 0.0009889 = 18.819130(20)$	217.81	0.108	0.2998(58)	10.7
$f_{39} + 0.0007039 = 26.864490(32)$	310.93	0.069	0.8513(90)	7.6
$f_0 + f_2 - 0.004371$		0.0600	0.7838	6.6
$2f_0 - 0.000098$		0.0890	0.4775	11.6
$f_1 + f_2 - 0.001198$		0.0450	0.7144	6.7
Theoretical frequency resolution: 0.00102 d^{-1}				
Zeropoint: 7.97601007 mag				
Residuals: 0.000991485736 mag				

Table 14
Frequency solution of CD-54 7154 (=TIC 173503902) based on *TESS* sectors 12 and 39. The digits in parentheses represent the error in the last two or three decimal places. The amplitude units are milli-magnitudes (mmag), with typical uncertainties of 0.0418 mmag. The previously detected frequencies are marked by asterisks.

Frequency (d^{-1})	μHz	Amplitude (mmag)	Phase (0-1)	SNR
$f_0 = *9.162285(01)$	106.04	24.388	0.0327(03)	461.0
$f_1 = *9.369020(02)$	108.44	15.4150	0.7847	291.4
$f_2 = *9.15744$	105.99	–	–	–
$f_3 = *9.15132$	105.92	–	–	–
$f_4 = *15.404979(12)$	178.30	2.431	0.9971(27)	62.3
$f_5 = 16.246765(19)$	188.04	1.589	0.3877(42)	34.7
$f_6 = 9.879882(23)$	114.35	1.317	0.6386(51)	27.3
$f_7 = 20.629477(53)$	238.77	0.566	0.5506(118)	14.4
$f_8 = 16.459082(53)$	190.50	0.568	0.6116(117)	12.4
$f_9 = 10.258152(59)$	118.73	0.514	0.3408(129)	10.6
$f_{10} = 15.427366(67)$	178.56	0.452	0.9713(147)	11.6
$f_{11} = 16.213636(70)$	187.66	0.430	0.8800(155)	9.4
$f_{12} = 19.408859(73)$	224.64	0.415	0.4193(160)	9.5
$f_{13} = 9.769503(77)$	113.07	0.389	0.3994(171)	8.1
$f_{14} = 17.375864(78)$	201.11	0.385	0.7853(173)	7.8
$f_{15} = 10.380897(85)$	120.15	0.353	0.3007(189)	7.3
$f_{16} = 14.695983(99)$	170.09	0.304	0.7244(219)	9.5
$f_{17} = f_0 - 0.02563 = 9.136657(14)$	105.75	2.213	0.6940(30)	41.8
$f_{18} = f_0 - 0.03359 = 9.128695(25)$	105.66	1.211	0.1088(55)	22.9
$f_{19} = f_0 + 0.02593 = 9.188212(34)$	106.35	0.881	0.3646(76)	16.7
Combination and dependent frequencies within resolution limit 0.0182 d^{-1}				
$f_{20} = f_0 + f_1 + 0.000117$	214.48	1.7470	0.3624	36.6
$f_{21} = 2f_0 - 0.002688$	212.12	1.0050	0.1237	21.1
$f_{22} = f_0 + f_1 - 0.00329$	214.44	0.7190	0.1536	15.1
$f_{23} = 2f_1 - 0.002688$	216.91	0.5990	0.5512	12.6
$f_{24} = f_0 + f_2 - 0.002691$	284.37	0.3220	0.9611	7.7
Frequency resolution: 0.00131 d^{-1}				
Zeropoint: 0.000301970746 mag				
Residuals: 0.00212318609 mag				

spectra can provide much better constraints on the control parameter of a stellar model, such as the initial chemical composition, mass, age, mixing-length, and opacity of the stellar material, etc.

One of the widely accepted excitation mechanisms for the low-frequency (0.3–5 d^{-1}) gravity-mode pulsations in γ Dor stars are driven by the modulation of the radiative flux by convection at the base of a deep envelope convection zone (Guzik et al., 2000). However, it is not the whole story because some γ Dor stars have been observed that also pulsates in δ Sct-type p-mode pulsations driven by the H and He ionization κ-effect. It is not known whether a single excitation mechanism can be responsible for both the p and g modes in hybrid δ Sct/γ Dor stars (Balona et al., 2015). A recent theoretic study shows that the oscillations of δ Sct and γ Dor stars are both due to the combination of the κ-mechanism and the coupling between convection and oscillations. These stars belong to the same class of variables at the low-luminosity part of the Cepheid instability strip. Within the δ Sct-γ Dor instability strip, most of the pulsating variables are very likely hybrids that are excited in both p and g modes (Xiong et al., 2016). High-precision photometry will reveal more hybrid pulsations, prompting an investigation into a possible unified pulsation mechanism. We are

Table 15
Frequency solution of GSC 04040-01606 based on *TESS* sectors 18, 24 and 25. The digits in parentheses represent the error in the last two or three decimal places. The amplitude units are milli-magnitudes (mmag), with typical uncertainties of 0.1542 mmag.

Frequency (d^{-1})	μHz	Amplitude (mmag)	Phase (0-1)	SNR
f_0 = 7.543132(53)	87.30	7.421	0.0950(33)	45.6
f_1 = 7.168275(65)	82.97	6.057	0.5795(41)	36.4
f_2 = 6.515472(184)	75.41	2.124	0.8685(116)	13.2
f_3 = 11.854332(333)	137.20	1.177	0.7561(208)	8.4
f_4 = 6.754491(372)	78.18	1.052	0.9157(233)	6.3
f_5 = 14.217330(378)	164.55	1.037	0.5742(237)	6.7
f_6 = 11.977436(412)	138.63	0.950	0.9333(258)	6.8
f_7 = 6.190357(445)	71.65	0.880	0.6625(279)	5.8
f_8 = 12.324753(476)	142.65	0.823	0.8473(298)	6.0
f_9 = 13.612377(484)	157.55	0.810	0.4309(303)	5.5
f_{10} = 6.500103(524)	75.23	0.747	0.5437(328)	4.7
f_{11} = 7.948547(539)	92.00	0.727	0.0347(337)	4.6
f_{12} = 14.442319(556)	167.16	0.705	0.5606(348)	4.5
f_{13} = 9.109439(610)	105.43	0.643	0.3949(382)	4.7

Effective frequency resolution of 0.0122 d^{-1}
Zeropoint: 0.9982993 mag
Residuals: 0.0058959 mag

looking into theoretic updates of the Hertzsprung-Russell diagram for stellar oscillations, which would be a revolutionary change from the earlier picture such as that by Christensen-Dalsgaard (1988).

CRediT authorship contribution statement

Ai-Ying Zhou: Writing – review & editing, Writing – original draft, Visualization, Validation, Supervision, Software, Resources, Project administration, Methodology, Investigation, Formal analysis, Data curation, Conceptualization.

Declaration of competing interest

The authors declare that they have no known competing financial interests or personal relationships that could have appeared to influence the work reported in this paper.

Data availability

Data will be made available on request.

Acknowledgments

I appreciate the anonymous referee for his/her thoughtful comments and suggestions which allowed the author to greatly improve the quality of the manuscript. I am indebted to my wife Jingyun Zhang for her unwavering support throughout my research. This work could not have been done without her continuous support. This paper includes data collected with the *TESS* mission (Ricker et al., 2015), obtained from the MAST data archive at the Space Telescope Science Institute (STScI). Funding for the *TESS* mission is provided by the NASA Explorer Program. STScI is operated by the Association of Universities for Research in Astronomy, Inc., under NASA contract NAS 5–26555. This paper includes data collected by the *Kepler* mission. Funding for the *Kepler* mission is provided by the NASA Science Mission Directorate. This paper also includes data collected by the K2 mission. Funding for the K2 mission is provided by the NASA Science Mission directorate. We acknowledge the use of *TESS* data, which are derived from pipelines at the *TESS* Science Processing Operations Centre (SPOC). *TESS* High Level Science Products (HLSP) produced by the Quick-Look Pipeline (QLP) at the *TESS* Science Office at MIT, which are publicly available from the Mikulski Archive for Space Telescopes (MAST). This research has made use of the SIMBAD/VizieR databases, operated at CDS, Strasbourg, France. This work has made use of data from the European Space Agency (ESA) mission *Gaia* (Gaia Collaboration et al., 2016b, https://www.cosmos.esa.int/gaia), processed by the *Gaia* Data Processing and Analysis Consortium (DPAC, https://www.cosmos.esa.int/web/gaia/dpac/consortium). Funding for the DPAC has been provided by national institutions, in particular, the institutions participating in the *Gaia* Multilateral Agreement. This work made use of *Astropy*: a community-developed core Python package and an ecosystem of tools and resources for astronomy (Astropy Collaboration et al., 2013, 2018, 2022); Astroquery (Ginsburg et al., 2019); Lightkurve (Lightkurve Collaboration et al., 2018); Matplotlib (Hunter, 2007); SciPy (Virtanen et al., 2020); NumPy (Harris et al., 2020).

References

Antoci, V., Cunha, M.S., Bowman, D.M., Murphy, S.J., Kurtz, D.W., Bedding, T.R., Borre, C.C., Christophe, S., Daszyńska-Daszkiewicz, J., Fox-Machado, L., García Hernández, A., Ghasemi, H., Handberg, R., Hansen, H., Hasanzadeh, A., Houdek, G., Johnston, C., Justesen, A.B., Kahraman Alicavus, F., Kotysz, K., Latham, D., Matthews, J.M., Mønster, J., Niemczura, E., Paunzen, E., Sánchez Arias, J.P., Pigulski, A., Pepper, J., Richey-Yowell, T., Safari, H., Seager, S., Smalley, B., Shutt, T., Sódor, A., Suárez, J.C., Tkachenko, A., Wu, T., Zwintz, K., Barceló Forteza, S., Brunsden, E., Bognár, Z., Buzasi, D.L., Chowdhury, S., De Cat, P., Evans, J.A., Guo, Z., Guzik, J.A., Jevtic, N., Lampens, P., Lares Martiz, M., Lovekin, C., Li, G., Mirouh, G.M., Mkrtichian, D., Monteiro, M.J.P.F.G., Nemec, J.M., Ouazzani, R.M., Pascual-Granado, J., Reese, D.R., Rieutord, M., Rodon, J.R., Skarka, M., Sowicka, P., Stateva, I., Szabó, R., Weiss, W.W., 2019. The first view of δ Scuti and γ Doradus stars with the TESS mission. Mon. Not. R. Astron. Soc. 490, 4040–4059. http://dx.doi.org/10.1093/mnras/stz2787, arXiv:1909.12018.

Arentoft, T., Kjeldsen, H., Nuspl, J., Bedding, T.R., Fronto, A., Viskum, M., Frandsen, S., Belmonte, J.A., 1998. Photometry and asteroseismology of delta Scuti stars in Praesepe. Astron. Astrophys. 338, 909–918.

Astropy Collaboration, Price-Whelan, A.M., Lim, P.L., Earl, N., Starkman, N., Bradley, L., Shupe, D.L., Patil, A.A., Corrales, L., Brasseur, C.E., Nöthe, M., Donath, A., Tollerud, E., Morris, B.M., Ginsburg, A., Vaher, E., Weaver, B.A., Tocknell, J., Jamieson, W., van Kerkwijk, M.H., Robitaille, T.P., Merry, B., Bachetti, M., Günther, H.M., Aldcroft, T.L., Alvarado-Montes, J.A., Archibald, A.M., Bódi, A., Bapat, S., Barentsen, G., Bazán, J., Biswas, M., Boquien, M., Burke, D.J., Cara, D., Cara, M., Conroy, K.E., Conseil, S., Craig, M.W., Cross, R.M., Cruz, K.L., D'Eugenio, F., Dencheva, N., Devillepoix, H.A.R., Dietrich, J.P., Eigenbrot, A.D., Erben, T., Ferreira, L., Foreman-Mackey, D., Fox, R., Freij, N., Garg, S., Geda, R., Glattly, L., Gondhalekar, Y., Gordon, K.D., Grant, D., Greenfield, P., Groener, A.M., Guest, S., Gurovich, S., Handberg, R., Hart, A., Hatfield-Dodds, Z., Homeier, D., Hosseinzadeh, G., Jenness, T., Jones, C.K., Joseph, P., Kalmbach, J.B., Karamehmetoglu, E., Kałuszyński, M., Kelley, M.S.P., Kern, N., Kerzendorf, W.E., Koch, E.W., Kulumani, S., Lee, A., Ly, C., Ma, Z., MacBride, C., Maljaars, J.M., Muna, D., Murphy, N.A., Norman, H., O'Steen, R., Oman, K.A., Pacifici, C., Pascual, S., Pascual-Granado, J., Patil, R.R., Perren, G.I., Pickering, T.E., Rastogi, T., Roulston, B.R., Ryan, D.F., Rykoff, E.S., Sabater, J., Sakurikar, P., Salgado, J., Sanghi, A., Saunders, N., Savchenko, V., Schwardt, L., Seifert-Eckert, M., Shih, A.Y., Jain, A.S., Shukla, G., Sick, J., Simpson, C., Singanamalla, S., Singer, L.P., Singhal, J., Sinha, M., Sipőcz, B.M., Spitler, L.R., Stansby, D., Streicher, O., Šumak, J., Swinbank, J.D., Taranu, D.S., Tewary, N., Tremblay, G.R., Val-Borro, M.d., Van Kooten, S.J., Vasović, Z., Verma, S., de Miranda Cardoso, J.V., Williams, P.K.G., Wilson, T.J., Winkel, B., Wood-Vasey, W.M., Xue, R., Yoachim, P., Zhang, C., Zonca, A., Astropy Project Contributors, 2022. The astropy project: Sustaining and growing a community-oriented open-source project and the latest major release (v5.0) of the core package. Astrophys. J. 935, 167. http://dx.doi.org/10.3847/1538-4357/ac7c74, arXiv:2206.14220.

Astropy Collaboration, Price-Whelan, A.M., Sipőcz, B.M., Günther, H.M., Lim, P.L., Crawford, S.M., Conseil, S., Shupe, D.L., Craig, M.W., Dencheva, N., Ginsburg, A., VanderPlas, J.T., Bradley, L.D., Pérez-Suárez, D., de Val-Borro, M., Aldcroft, T.L., Cruz, K.L., Robitaille, T.P., Tollerud, E.J., Ardelean, C., Babej, T., Bach, Y.P., Bachetti, M., Bakanov, A.V., Bamford, S.P., Barentsen, G., Barmby, P., Baumbach, A., Berry, K.L., Biscani, F., Boquien, M., Bostroem, K.A., Bouma, L.G., Brammer, G.B., Bray, E.M., Breytenbach, H., Buddelmeijer, H., Burke, D.J., Calderone, G., Cano Rodríguez, J.L., Cara, M., Cardoso, J.V.M., Cheedella, S., Copin, Y., Corrales, L., Crichton, D., D'Avella, D., Deil, C., Depagne, É., Dietrich, J.P., Donath, A., Droettboom, M., Earl, N., Erben, T., Fabbro, S., Ferreira, L.A., Finethy, T., Fox, R.T., Garrison, L.H., Gibbons, S.L.J., Goldstein, D.A., Gommers, R., Greco, J.P., Greenfield, P., Groener, A.M., Grollier, F., Hagen, A., Hirst, P., Homeier, D., Horton, A.J., Hosseinzadeh, G., Hu, L., Hunkeler, J.S., Ivezić, Ž., Jain, A., Jenness, T., Kanarek, G., Kendrew, S., Kern, N.S., Kerzendorf, W.E., Khvalko, A., King, J., Kirkby, D., Kulkarni, A.M., Kumar, A., Lee, A., Lenz, D., Littlefair, S.P., Ma, Z., Macleod, D.M., Mastropietro, M., McCully, C., Montagnac, S., Morris, B.M., Mueller, M., Mumford, S.J., Muna, D., Murphy, N.A., Nelson, S., Nguyen, G.H., Ninan, J.P., Nöthe, M., Ogaz, S., Oh, S., Parejko, J.K., Parley, N., Pascual, S., Patil, R., Patil, A.A., Plunkett, A.L., Prochaska, J.X., Rastogi, T.,

Reddy Janga, V., Sabater, J., Sakurikar, P., Seifert, M., Sherbert, L.E., Sherwood-Taylor, H., Shih, A.Y., Sick, J., Silbiger, M.T., Singanamalla, S., Singer, L.P., Sladen, P.H., Sooley, K.A., Sornarajah, S., Streicher, O., Teuben, P., Thomas, S.W., Tremblay, G.R., Turner, J.E.H., Terrón, V., van Kerkwijk, M.H., de l Vega, A., Watkins, L.L., Weaver, B.A., Whitmore, J.B., Woillez, J., Zabalza, V., Astropy Contributors, 2018. The astropy project: Building an open-science project and status of the v2.0 core package. Astron. J. 156, 123. http://dx.doi.org/10.3847/1538-3881/aabc4f, arXiv:1801.02634.

Astropy Collaboration, Robitaille, T.P., Tollerud, E.J., Greenfield, P., Droettboom, M., Bray, E., Aldcroft, T., Davis, M., Ginsburg, A., Price-Whelan, A.M., Kerzendorf, W.E., Conley, A., Crighton, N., Barbary, K., Muna, D., Ferguson, H., Grollier, F., Parikh, M.M., Nair, P.H., Unther, H.M., Deil, C., Woillez, J., Conseil, S., Kramer, R., Turner, J.E.H., Singer, L., Fox, R., Weaver, B.A., Zabalza, V., Edwards, Z.I., Azalee Bostroem, K., Burke, D.J., Casey, A.R., Crawford, S.M., Dencheva, N., Ely, J., Jenness, T., Labrie, K., Lim, P.L., Pierfederici, F., Pontzen, A., Ptak, A., Refsdal, B., Servillat, M., Streicher, O., 2013. Astropy: A community Python package for astronomy. Astron. Astrophys. 558, A33. http://dx.doi.org/10.1051/0004-6361/201322068, arXiv:1307.6212.

Balona, L.A., Daszyńska-Daszkiewicz, J., Pamyatnykh, A.A., 2015. Pulsation frequency distribution in δ Scuti stars. Mon. Not. R. Astron. Soc. 452, 3073–3084. http://dx.doi.org/10.1093/mnras/stv1513, arXiv:1505.07216.

Battley, M.P., Kunimoto, M., Armstrong, D.J., Pollacco, D., 2021. Revisiting the Kepler field with TESS: Improved ephemerides using TESS 2 min data. Mon. Not. R. Astron. Soc. 503, 4092–4104. http://dx.doi.org/10.1093/mnras/stab701, arXiv:2103.03259.

Bedding, T.R., Murphy, S.J., Crawford, C., Hey, D.R., Huber, D., Kjeldsen, H., Li, Y., Mann, A.W., Torres, G., White, T.R., Zhou, G., 2023. TESS observations of the pleiades cluster: A nursery for δ Scuti stars. Astrophys. J. Lett. 946, L10. http://dx.doi.org/10.3847/2041-8213/acc17a, arXiv:2212.12087.

Bedding, T.R., Murphy, S.J., Hey, D.R., Huber, D., Li, T., Smalley, B., Stello, D., White, T.R., Ball, W.H., Chaplin, W.J., Colman, I.L., Fuller, J., Gaidos, E., Harbeck, D.R., Hermes, J.J., Holdsworth, D.L., Li, G., Li, Y., Mann, A.W., Reese, D.R., Sekaran, S., Yu, J., Antoci, V., Bergmann, C., Brown, T.M., Howard, A.W., Ireland, .M.J., Isaacson, H., Jenkins, J.M., Kjeldsen, H., McCully, C., Rabus, M., Rains, A.D., Ricker, G.R., Tinney, C.G., Vanderspek, R.K., 2020. Very regular high-frequency pulsation modes in young intermediate-mass stars. Nature 581, 147–151. http://dx.doi.org/10.1038/s41586-020-2226-8, arXiv:2005.06157.

Bowman, D.M., Kurtz, D.W., Breger, M., Murphy, S.J., Holdsworth, D.L., 2016. Amplitude modulation in δ Sct stars: statistics from an ensemble study of Kepler targets. Mon. Not. R. Astron. Soc. 460, 1970–1989. http://dx.doi.org/10.1093/mnras/stw1153, arXiv:1605.03955.

Breger, M., Stich, J., Garrido, R., Martin, B., Jiang, S.Y., Li, Z.P., Hube, D.P., Ostermann, W., Paparo, M., Scheck, M., 1993. Nonradial pulsation of the delta Scuti star BU CANCRI in the Praesepe cluster. Astron. Astrophys. 271, 482–486.

Bruntt, H., Stello, D., Suárez, J.C., Arentoft, T., Bedding, T.R., Bouzid, M.Y., Csubry, Z., Dall, T.H., Dind, Z.E., Frandsen, S., Gilliland, R.L., Jacob, A.P., Jensen, H.R., Kang, Y.B., Kim, S.L., Kiss, L.L., Kjeldsen, H., Koo, J.R., Lee, J.A., Lee, C.U., Nuspl, J., Sterken, C., Szabó, R., 2007. Multisite campaign on the open cluster M67 - III. δ Scuti pulsations in the blue stragglers. Mon. Not. R. Astron. Soc. 378, 1371–1384. http://dx.doi.org/10.1111/j.1365-2966.2007.11865.x, arXiv:0704.3884.

Buchler, J.R., Kolláth, Z., 2011. On the blazhko effect in RR lyrae stars. Astrophys. J. 731, 24. http://dx.doi.org/10.1088/0004-637X/731/1/24, arXiv:1101.1502.

Christensen-Dalsgaard, J., 1988. A Hertzsprung-Russell diagram for stellar oscillations. In: Christensen-Dalsgaard, J., Frandsen, S. (Eds.), Advances in Helio- and Asteroseismology. p. 295.

Demory, B.O., Pozuelos, F.J., Gómez Maqueo Chew, Y., Sabin, L., Petrucci, R., Schroffenegger, U., Grimm, S.L., Sestovic, M., Gillon, M., McCormac, J., Barkaoui, K., Benz, W., Bieryla, A., Bouchy, F., Burdanov, A., Collins, K.A., de Wit, J., Dressing, C.D., Garcia, L.J., Giacalone, S., Guerra, P., Haldemann, J., Heng, K., Jehin, E., Jofré, E., Kane, S.R., Lillo-Box, J., Maigné, V., Mordasini, C., Morris, B.M., Niraula, P., Queloz, D., Rackham, B.V., Savel, A.B., Soubkiou, A., Srdoc, G., Stassun, K.G., Triaud, A.H.M.J., Zambelli, R., Ricker, G., Latham, D.W., Seager, S., Winn, J.N., Jenkins, J.M., Calvario-Velásquez, T., Franco Herrera, J.A., Colorado, E., Cadena Zepeda, E.O., Figueroa, L., Watson, A.M., Lugo-Ibarra, E.E., Carigi, L., Guisa, G., Herrera, J., Sierra Díaz, G., Suárez, J.C., Barrado, D., Batalha, N.M., Benkhaldoun, Z., Chontos, A., Dai, F., Essack, Z., Ghachoui, M., Huang, C.X., Huber, D., Isaacson, H., Lissauer, J.J., Morales-Calderón, M., Robertson, P., Roy, A., Twicken, J.D., Vanderburg, A., Weiss, L.M., 2020. A super-Earth and a sub-Neptune orbiting the bright, quiet M3 dwarf TOI-1266. Astron. Astrophys. 642, A49. http://dx.doi.org/10.1051/0004-6361/202038616, arXiv:2009.04317.

Du, B.T., Zhou, A.Y., Zhang, X.B., Liu, Z.L., Zhang, R.X., Li, H.B., Jinag, Z.J., Dong, X.Y., Zhao, L.M., 1999. A newly Discovered Delta scuti variable star. Inf. Bull. Var. Stars 4805, 1.

Dumusque, X., Turner, O., Dorn, C., Eastman, J.D., Allart, R., Adibekyan, V., Sousa, S., Santos, N.C., Mordasini, C., Bourrier, V., Bouchy, F., Coffinet, A., Davies, M.D., Díaz, R.F., Fausnaugh, M.M., Glidden, A., Guerrero, N., Henze, C.E., Jenkins, J.M., Latham, D.W., Lovis, C., Mayor, M., Pepe, F., Quintana, E.V., Ricker, G.R., Rowden, P., Segransan, D., Suárez Mascareño, A., Seager, S., Twicken, J.D., Udry, S., Vanderspek, R.K., Winn, J.N., 2019. Hot, rocky and warm, puffy super-Earths orbiting TOI-402 (HD 15337). Astron. Astrophys. 627, A43. http://dx.doi.org/10.1051/0004-6361/201935457, arXiv:1903.05419.

Gaia Collaboration, Prusti, T., de Bruijne, J.H.J., Brown, A.G.A., Vallenari, A., Babusiaux, C., Bailer-Jones, C.A.L., Bastian, U., Biermann, M., Evans, D.W., Eyer, L., Jansen, F., Jordi, C., Klioner, S.A., Lammers, U., Lindegren, L., Luri, X., Mignard, F., Milligan, D.J., Panem, C., Poinsignon, V., Pourbaix, D., Randich, S., Sarri, G., Sartoretti, P., Siddiqui, H.I., Soubiran, C., Valette, V., van Leeuwen, F., Walton, N.A., Aerts, C., Arenou, F., Cropper, M., Drimmel, R., Høg, E., Katz, D., Lattanzi, M.G., O'Mullane, W., Grebel, E.K., Holland, A.D., Huc, C., Passot, X., Bramante, L., Cacciari, C., Castañeda, J., Chaoul, L., Cheek, N., De Angeli, F., Fabricius, C., Guerra, R., Hernández, J., Jean-Antoine-Piccolo, A., Masana, E., Messineo, R., Mowlavi, N., Nienartowicz, K., Ordóñez-Blanco, D., Panuzzo, P., Portell, J., Richards, P.J., Riello, M., Seabroke, G.M., Tanga, P., Thévenin, F., Torra, J., Els, S.G., Gracia-Abril, G., Comoretto, G., Garcia-Reinaldos, M., Lock, T., Mercier, E., Altmann, M., Andrae, R., Astraatmadja, T.L., Bellas-Velidis, I., Benson, K., Berthier, J., Blomme, R., Busso, G., Carry, B., Cellino, A., Clementini, G., Cowell, S., Creevey, O., Cuypers, J., Davidson, M., De Ridder, J., de Torres, A., Delchambre, L., Dell'Oro, A., Ducourant, C., Frémat, Y., García-Torres, M., Gosset, E., Halbwachs, J.L., Hambly, N.C., Harrison, D.L., Hauser, M., Hestroffer, D., Hodgkin, S.T., Huckle, H.E., Hutton, A., Jasniewicz, G., Jordan, S., Kontizas, M., Korn, A.J., Lanzafame, A.C., Manteiga, M., Moitinho, A., Muinonen, K., Osinde, J., Pancino, E., Pauwels, T., Petit, J.M., Recio-Blanco, A., Robin, A.C., Sarro, L.M., Siopis, C., Smith, M., Smith, K.W., Sozzetti, A., Thuillot, W., van Reeven, W., Viala, Y., Abbas, U., Abreu Aramburu, A., Accart, S., Aguado, J.J., Allan, P.M., Allasia, W., Altavilla, G., Álvarez, M.A., Alves, J., Anderson, R.I., Andrei, A.H., Anglada Varela, E., Antiche, E., Antoja, T., Antón, S., Arcay, B., Atzei, A., Ayache, L., Bach, N., Baker, S.G., Balaguer-Núñez, L., Barache, C., Barata, C., Barbier, A., Barblan, F., Baroni, M., Barrado y Navascués, D., Barros, M., Barstow, M.A., Becciani, U., Bellazzini, M., Bellei, G., Bello García, A., Belokurov, V., Bendjoya, P., Berihuete, A., Bianchi, L., Bienaymé, O., Billebaud, F., Blagorodnova, N., Blanco-Cuaresma, S., Boch, T., Bombrun, A., Borrachero, R., Bouquillon, S., Bourda, G., Bouy, H., Bragaglia, A., Breddels, M.A., Brouillet, N., Brüsemeister, T., Bucciarelli, B., Budnik, F., Burgess, P., Burgon, R., Burlacu, A., Busonero, D., Buzzi, R., Caffau, E., Cambras, J., Campbell, H., Cancelliere, R., Cantat-Gaudin, T., Carlucci, T., Carrasco, J.M., Castellani, M., Charlot, P., Charnas, J., Charvet, P., Chassat, F., Chiavassa, A., Clotet, M., Cocozza, G., Collins, R.S., Collins, P., Costigan, G., Crifo, F., Cross, N.J.G., Crosta, M., Crowley, C., Dafonte, C., Damerdji, Y., Dapergolas, A., David, P., David, M., De Cat, P., de Felice, F., de Laverny, P., De Luise, F., De March, R., de Martino, D., de Souza, R., Debosscher, J., del Pozo, E., Delbo, M., Delgado, A., Delgado, H.E., di Marco, F., Di Matteo, P., Diakite, S., Distefano, E., Dolding, C., Dos Anjos, S., Drazinos, P., Durán, J., Dzigan, Y., Ecale, E., Edvardsson, B., Enke, H., Erdmann, M., Escolar, D., Espina, M., Evans, N.W., Eynard Bontemps, G., Fabre, C., Fabrizio, M., Faigler, S., Falcão, A.J., Farràs Casas, M., Faye, F., Federici, L., Fedorets, G., Fernández-Hernández, J., Fernique, P., Fienga, A., Figueras, F., Filippi, F., Findeisen, K., Fonti, A., Fouesneau, M., Fraile, E., Fraser, M., Fuchs, J., Furnell, R., Gai, M., Galleti, S., Galluccio, L., Garabato, D., García-Sedano, F., Garé, P., Garofalo, A., Garralda, N., Gavras, P., Gerssen, J., Geyer, R., Gilmore, G., Girona, S., Giuffrida, G., Gomes, M., González-Marcos, A., González-Núñez, J., González-Vidal, J.J., Granvik, M., Guerrier, A., Guillout, P., Guiraud, J., Gúrpide, A., Gutiérrez-Sánchez, R., Guy, L.P., Haigron, R., Hatzidimitriou, D., Haywood, M., Heiter, U., Helmi, A., Hobbs, D., Hofmann, W., Holl, B., Holland, G., Hunt, J.A.S., Hypki, A., Icardi, V., Irwin, M., Jevardat de Fombelle, G., Jofré, P., Jonker, P.G., Jorissen, A., Julbe, F., Karampelas, A., Kochoska, A., Kohley, R., Kolenberg, K., Kontizas, E., Koposov, S.E., Kordopatis, G., Koubsky, P., Kowalczyk, A., Krone-Martins, A., Kudryashova, M., Kull, I., Bachchan, R.K., Lacoste-Seris, F., Lanza, A.F., Lavigne, J.B., Le Poncin-Lafitte, C., Lebreton, Y., Lebzelter, T., Leccia, S., Leclerc, N., Lecoeur-Taibi, I., Lemaitre, V., Lenhardt, H., Leroux, F., Liao, S., Licata, E., Lindstrøm, H.E.P., Lister, T.A., Livanou, E., Lobel, A., Löffler, W., López, M., Lopez-Lozano, A., Lorenz, D., Loureiro, T., MacDonald, I., Magalhães Fernandes, T., Managau, S., Mann, R.G., Mantelet, G., Marchal, O., Marchant, J.M., Marconi, M., Marie, J., Marinoni, S., Marrese, P.M., Marschalkó, G., Marshall, D.J., Martín-Fleitas, J.M., Martino, M., Mary, N., Matijevič, G., Mazeh, T., McMillan, P.J., Messina, S., Mestre, A., Michalik, D., Millar, N.R., Miranda, B.M.H., Molina, D., Molinaro, R., Molinaro, M., Molnár, L., Moniez, M., Montegriffo, P., Monteiro, D., Mor, R., Mora, A., Morbidelli, R., Morel, T., Morgenthaler, S., Morley, T., Morris, D., Mulone, A.F., Muraveva, T., Musella, I., Narbonne, J., Nelemans, G., Nicastro, L., Noval, L., Ordénovic, C., Ordieres-Meré, J., Osborne, P., Pagani, C., Pagano, I., Pailler, F., Palacin, H., Palaversa, L., Parsons, P., Paulsen, T., Pecoraro, M., Pedrosa, R., Pentikäinen, H., Pereira, J., Pichon, B., Piersimoni, A.M., Pineau, F.X., Plachy, E., Plum, G., Poujoulet, E., Prša, A., Pulone, L., Ragaini, S., Rago, S., Rambaux, N., Ramos-Lerate, M., Ranalli, P., Rauw, G., Read, A., Regibo, S., Renk, F., Reylé, C., Ribeiro, R.A., Rimoldini, L., Ripepi, V., Riva, A., Rixon, G., Roelens, M., Romero-Gómez, M., Rowell, N., Royer, F., Rudolph, A., Ruiz-Dern, L., Sadowski, G., Sagristà Sellés, T., Sahlmann, J., Salgado, J., Salguero, E., Sarasso, M., Savietto, H., Schnorhk, A., Schultheis, M., Sciacca, E., Segol, M., Segovia, J.C., Segransan, D., Serpell, E., Shih, I.C., Smareglia, R., Smart, R.L., Smith, C., Solano, E., Solitro, F., Sordo, R., Soria Nieto, S., Souchay, J., Spagna, A., Spoto, F., Stampa, U., Steele, I.A., Steidelmüller, H., Stephenson, C.A., Stoev, H., Suess, F.F., Süveges, M., Surdej, J., Szabados, L., Szegedi-Elek, E., Tapiador, D., Taris, F., Tauran, G., Taylor, M.B., Teixeira, R., Terrett, D., Tingley, B., Trager, S.C., Turon, C., Ulla, A., Utrilla, E., Valentini, G., van Elteren, A., Van Hemelryck, E., van Leeuwen, M., Varadi, M., Vecchiato, A., Veljanoski, J., Via, T., Vicente, D., Vogt, S., Voss, H., Votruba, V., Voutsinas, S., Walmsley, G., Weiler, M., Weingrill, K., Werner, D.,

Wevers, T., Whitehead, G., Wyrzykowski, Ł., Yoldas, A., Žerjal, M., Zucker, S., Zurbach, C., Zwitter, T., Alecu, A., Allen, M., Allende Prieto, C., Amorim, A., Anglada-Escudé, G., Arsenijevic, V., Azaz, S., Balm, P., Beck, M., Bernstein, H.H., Bigot, L., Bijaoui, A., Blasco, C., Bonfigli, M., Bono, G., Boudreault, S., Bressan, A., Brown, S., Brunet, P.M., Bunclark, P., Buonanno, R., Butkevich, A.G., Carret, C., Carrion, C., Chemin, L., Chéreau, F., Corcione, L., Darmigny, E., de Boer, K.S., de Teodoro, P., de Zeeuw, P.T., Delle Luche, C., Domingues, C.D., Dubath, P., Fodor, F., Frézouls, B., Fries, A., Fustes, D., Fyfe, D., Gallardo, E., Gallegos, J., Gardiol, D., Gebran, M., Gomboc, A., Gómez, A., Grux, E., Gueguen, A., Heyrovsky, A., Hoar, J., Iannicola, G., Isasi Parache, Y., Janotto, A.M., Joliet, E., Jonckheere, A., Keil, R., Kim, D.W., Klagyivik, P., Klar, J., Knude, J., Kochukhov, O., Kolka, I., Kos, J., Kutka, A., Lainey, V., LeBouquin, D., Liu, C., Loreggia, D., Makarov, V.V., Marseille, M.G., Martayan, C., Martinez-Rubi, O., Massart, B., Meynadier, F., Mignot, S., Munari, U., Nguyen, A.T., Nordlander, T., Ocvirk, P., O'Flaherty, K.S., Olias Sanz, A., Ortiz, P., Osorio, J., Oszkiewicz, D., Ouzounis, A., Palmer, M., Park, P., Pasquato, E., Peltzer, C., Peralta, J., 2016a. The Gaia mission. Astron. Astrophys. 595, A1. http://dx.doi.org/10.1051/0004-6361/201629272, arXiv:1609.04153.

Gaia Collaboration, Prusti, T., de Bruijne, J.H.J., Brown, A.G.A., Vallenari, A., Babusiaux, C., Bailer-Jones, C.A.L., Bastian, U., Biermann, M., Evans, D.W., Eyer, L., Jansen, F., Jordi, C., Klioner, S.A., Lammers, U., Lindegren, L., Luri, X., Mignard, F., Milligan, D.J., Panem, C., Poinsignon, V., Pourbaix, D., Randich, S., Sarri, G., Sartoretti, P., Siddiqui, H.I., Soubiran, C., Valette, V., van Leeuwen, F., Walton, N.A., Aerts, C., Arenou, F., Cropper, M., Drimmel, R., Høg, E., Katz, D., Lattanzi, M.G., O'Mullane, W., Grebel, E.K., Holland, A.D., Huc, C., Passot, X., Bramante, L., Cacciari, C., Castañeda, J., Chaoul, L., Cheek, N., De Angeli, F., Fabricius, C., Guerra, R., Hernández, J., Jean-Antoine-Piccolo, A., Masana, E., Messineo, R., Mowlavi, N., Nienartowicz, K., Ordóñez-Blanco, D., Panuzzo, P., Portell, J., Richards, P.J., Riello, M., Seabroke, G.M., Tanga, P., Thévenin, F., Torra, J., Els, S.G., Gracia-Abril, G., Comoretto, G., Garcia-Reinaldos, M., Lock, T., Mercier, E., Altmann, M., Andrae, R., Astraatmadja, T.L., Bellas-Velidis, I., Benson, K., Berthier, J., Blomme, R., Busso, G., Carry, B., Cellino, A., Clementini, G., Cowell, S., Creevey, O., Cuypers, J., Davidson, M., De Ridder, J., de Torres, A., Delchambre, L., Dell'Oro, A., Ducourant, C., Frémat, Y., García-Torres, M., Gosset, E., Halbwachs, J.L., Hambly, N.C., Harrison, D.L., Hauser, M., Hestroffer, D., Hodgkin, S.T., Huckle, H.E., Hutton, A., Jasniewicz, G., Jordan, S., Kontizas, M., Korn, A.J., Lanzafame, A.C., Manteiga, M., Moitinho, A., Muinonen, K., Osinde, J., Pancino, E., Pauwels, T., Petit, J.M., Recio-Blanco, A., Robin, A.C., Sarro, L.M., Siopis, C., Smith, M., Smith, K.W., Sozzetti, A., Thuillot, W., van Reeven, W., Viala, Y., Abbas, U., Abreu Aramburu, A., Accart, S., Aguado, J.J., Allan, P.M., Allasia, W., Altavilla, G., Álvarez, M.A., Alves, J., Anderson, R.I., Andrei, A.H., Anglada Varela, E., Antiche, E., Antoja, T., Antón, S., Arcay, B., Atzei, A., Ayache, L., Bach, N., Baker, S.G., Balaguer-Núñez, L., Barache, C., Barata, C., Barbier, A., Barblan, F., Baroni, M., Barrado y Navascués, D., Barros, M., Barstow, M.A., Becciani, U., Bellazzini, M., Bellei, G., Bello García, , A., Belokurov, V., Bendjoya, P., Berihuete, A., Bianchi, L., Bienaymé, O., Billebaud, F., Blagorodnova, N., Blanco-Cuaresma, S., Boch, T., Bombrun, A., Borrachero, R., Bouquillon, S., Bourda, G., Bouy, H., Bragaglia, A., Breddels, M.A., Brouillet, N., Brüsemeister, T., Bucciarelli, B., Budnik, F., Burgess, P., Burgon, R., Burlacu, A., Busonero, D., Buzzi, R., Caffau, E., Cambras, J., Campbell, H., Cancelliere, R., Cantat-Gaudin, T., Carlucci, T., Carrasco, J.M., Castellani, M., Charlot, P., Charnas, J., Charvet, P., Chassat, F., Chiavassa, A., Clotet, M., Cocozza, G., Collins, R.S., Collins, P., Costigan, G., Crifo, F., Cross, N.J.G., Crosta, M., Crowley, C., Dafonte, C., Damerdji, Y., Dapergolas, A., David, P., David, M., De Cat, P., de Felice, F., de Laverny, P., De Luise, F., De March, R., de Martino, D., de Souza, R., Debosscher, J., del Pozo, E., Delbo, M., Delgado, A., Delgado, H.E., di Marco, F., Di Matteo, P., Diakite, S., Distefano, E., Dolding, C., Dos Anjos, S., Drazinos, P., Durán, J., Dzigan, Y., Ecale, E., Edvardsson, B., Enke, H., Erdmann, M., Escolar, D., Espina, M., Evans, N.W., Eynard Bontemps, G., Fabre, C., Fabrizio, M., Faigler, S., Falcão, A.J., Farràs Casas, M., Faye, F., Federici, L., Fedorets, G., Fernández-Hernández, J., Fernique, P., Fienga, A., Figueras, F., Filippi, F., Findeisen, K., Fonti, A., Fouesneau, M., Fraile, E., Fraser, M., Fuchs, J., Furnell, R., Gai, M., Galleti, S., Galluccio, L., Garabato, D., García-Sedano, F., Garé, P., Garofalo, A., Garralda, N., Gavras, P., Gerssen, J., Geyer, R., Gilmore, G., Girona, S., Giuffrida, G., Gomes, M., González-Marcos, A., González-Núñez, J., González-Vidal, J.J., Granvik, M., Guerrier, A., Guillout, P., Guiraud, J., Gúrpide, A., Gutiérrez-Sánchez, R., Guy, L.P., Haigron, R., Hatzidimitriou, D., Haywood, M., Heiter, U., Helmi, A., Hobbs, D., Hofmann, W., Holl, B., Holland, G., Hunt, J.A.S., Hypki, A., Icardi, V., Irwin, M., Jevardat de Fombelle, G., Jofré, P., Jonker, P.G., Jorissen, A., Julbe, F., Karampelas, A., Kochoska, A., Kohley, R., Kolenberg, K., Kontizas, E., Koposov, S.E., Kordopatis, G., Koubsky, P., Kowalczyk, A., Krone-Martins, A., Kudryashova, M., Kull, I., Bachchan, R.K., Lacoste-Seris, F., Lanza, A.F., Lavigne, J.B., Le Poncin-Lafitte, C., Lebreton, Y., Lebzelter, T., Leccia, S., Leclerc, N., Lecoeur-Taibi, I., Lemaitre, V., Lenhardt, H., Leroux, F., Liao, S., Licata, E., Lindstrøm, H.E.P., Lister, T.A., Livanou, E., Lobel, A., Löffler, W., López, M., Lopez-Lozano, A., Lorenz, D., Loureiro, T., MacDonald, I., Magalhães Fernandes, T., Managau, S., Mann, R.G., Mantelet, G., Marchal, O., Marchant, J.M., Marconi, M., Marie, J., Marinoni, S., Marrese, P.M., Marschalkó, G., Marshall, D.J., Martín-Fleitas, J.M., Martino, M., Mary, N., Matijevič, G., Mazeh, T., McMillan, P.J., Messina, S., Mestre, A., Michalik, D., Millar, N.R., Miranda, B.M.H., Molina, D., Molinaro, R., Molinaro, M., Molnár, L., Moniez, M., Montegriffo, P., Monteiro, D., Mor, R., Mora, A., Morbidelli, R., Morel, T., Morgenthaler, S., Morley, T., Morris, D., Mulone, A.F., Muraveva, T., Musella, I., Narbonne, J., Nelemans, G., Nicastro, L., Noval, L., Ordénovic, C., Ordieres-Meré, J., Osborne, P., Pagani, C., Pagano, I., Pailler, F., Palacin, H., Palaversa, L., Parsons, P., Paulsen, T., Pecoraro, M., Pedrosa, R., Pentikäinen, H., Pereira, J., Pichon, B., Piersimoni, A.M., Pineau, F.X., Plachy, E., Plum, G., Poujoulet, E., Prša, A., Pulone, L., Ragaini, S., Rago, S., Rambaux, N., Ramos-Lerate, M., Ranalli, P., Rauw, G., Read, A., Regibo, S., Renk, F., Reylé, C., Ribeiro, R.A., Rimoldini, L., Ripepi, V., Riva, A., Rixon, G., Roelens, M., Romero-Gómez, M., Rowell, N., Royer, F., Rudolph, A., Ruiz-Dern, L., Sadowski, G., Sagristà Sellés, T., Sahlmann, J., Salgado, J., Salguero, E., Sarasso, M., Savietto, H., Schnorhk, A., Schultheis, M., Sciacca, E., Segol, M., Segovia, J.C., Segransan, D., Serpell, E., Shih, I.C., Smareglia, R., Smart, R.L., Smith, C., Solano, E., Solitro, F., Sordo, R., Soria Nieto, S., Souchay, J., Spagna, A., Spoto, F., Stampa, U., Steele, I.A., Steidelmüller, H., Stephenson, C.A., Stoev, H., Suess, F.F., Süveges, M., Surdej, J., Szabados, L., Szegedi-Elek, E., Tapiador, D., Taris, F., Tauran, G., Taylor, M.B., Teixeira, R., Terrett, D., Tingley, B., Trager, S.C., Turon, C., Ulla, A., Utrilla, E., Valentini, G., van Elteren, A., Van Hemelryck, E., van Leeuwen, M., Varadi, M., Vecchiato, A., Veljanoski, J., Via, T., Vicente, D., Vogt, S., Voss, H., Votruba, V., Voutsinas, S., Walmsley, G., Weiler, M., Weingrill, K., Werner, D., Wevers, T., Whitehead, G., Wyrzykowski, Ł., Yoldas, A., Žerjal, M., Zucker, S., Zurbach, C., Zwitter, T., Alecu, A., Allen, M., Allende Prieto, C., Amorim, A., Anglada-Escudé, G., Arsenijevic, V., Azaz, S., Balm, P., Beck, M., Bernstein, H.H., Bigot, L., Bijaoui, A., Blasco, C., Bonfigli, M., Bono, G., Boudreault, S., Bressan, A., Brown, S., Brunet, P.M., Bunclark, P., Buonanno, R., Butkevich, A.G., Carret, C., Carrion, C., Chemin, L., Chéreau, F., Corcione, L., Darmigny, E., de Boer, K.S., de Teodoro, P., de Zeeuw, P.T., Delle Luche, C., Domingues, C.D., Dubath, P., Fodor, F., Frézouls, B., Fries, A., Fustes, D., Fyfe, D., Gallardo, E., Gallegos, J., Gardiol, D., Gebran, M., Gomboc, A., Gómez, A., Grux, E., Gueguen, A., Heyrovsky, A., Hoar, J., Iannicola, G., Isasi Parache, Y., Janotto, A.M., Joliet, E., Jonckheere, A., Keil, R., Kim, D.W., Klagyivik, P., Klar, J., Knude, J., Kochukhov, O., Kolka, I., Kos, J., Kutka, A., Lainey, V., LeBouquin, D., Liu, C., Loreggia, D., Makarov, V.V., Marseille, M.G., Martayan, C., Martinez-Rubi, O., Massart, B., Meynadier, F., Mignot, S., Munari, U., Nguyen, A.T., Nordlander, T., Ocvirk, P., O'Flaherty, K.S., Olias Sanz, A., Ortiz, P., Osorio, J., Oszkiewicz, D., Ouzounis, A., Palmer, M., Park, P., Pasquato, E., Peltzer, C., Peralta, J., 2016b. The Gaia mission. Astron. Astrophys. 595, A1. http://dx.doi.org/10.1051/0004-6361/201629272, arXiv:1609.04153.

Gaia Collaboration, Vallenari, A., Brown, A.G.A., Prusti, T., de Bruijne, J.H.J., Arenou, F., Babusiaux, C., Biermann, M., Creevey, O.L., Ducourant, C., Evans, D.W., Eyer, L., Guerra, R., Hutton, A., Jordi, C., Klioner, S.A., Lammers, U.L., Lindegren, L., Luri, X., Mignard, F., Panem, C., Pourbaix, D., Randich, S., Sartoretti, P., Soubiran, C., Tanga, P., Walton, N.A., Bailer-Jones, C.A.L., Bastian, U., Drimmel, R., Jansen, F., Katz, D., Lattanzi, M.G., van Leeuwen, F., Bakker, J., Cacciari, C., Castañeda, J., De Angeli, F., Fabricius, C., Fouesneau, M., Frémat, Y., Galluccio, L., Guerrier, A., Heiter, U., Masana, E., Messineo, R., Mowlavi, N., Nicolas, C., Nienartowicz, K., Pailler, F., Panuzzo, P., Riclet, F., Roux, W., Seabroke, G.M., Sordo, R., Thévenin, F., Gracia-Abril, G., Portell, J., Teyssier, D., Altmann, M., Andrae, R., Audard, M., Bellas-Velidis, I., Benson, K., Berthier, J., Blomme, R., Burgess, P.W., Busonero, D., Busso, G., Cánovas, H., Carry, B., Cellino, A., Cheek, N., Clementini, G., Damerdji, Y., Davidson, M., de Teodoro, P., Nuñez Campos, M., Delchambre, L., Dell'Oro, A., Esquej, P., Fernández-Hernández, J., Fraile, E., Garabato, D., García-Lario, P., Gosset, E., Haigron, R., Halbwachs, J.L., Hambly, N.C., Harrison, D.L., Hernández, J., Hestroffer, D., Hodgkin, S.T., Holl, B., Janßen, K., Jevardat de Fombelle, G., Jordan, S., Krone-Martins, A., Lanzafame, A.C., Löffler, W., Marchal, O., Marrese, P.M., Moitinho, A., Muinonen, K., Osborne, P., Pancino, E., Pauwels, T., Recio-Blanco, A., Reylé, C., Riello, M., Rimoldini, L., Roegiers, T., Rybizki, J., Sarro, L.M., Siopis, C., Smith, M., Sozzetti, A., Utrilla, E., van Leeuwen, M., Abbas, U., Ábrahám, P., Abreu Aramburu, A., Aerts, C., Aguado, J.J., Ajaj, M., Aldea-Montero, F., Altavilla, G., Álvarez, M.A., Alves, J., Anders, F., Anderson, R.I., Anglada Varela, E., Antoja, T., Baines, D., Baker, S.G., Balaguer-Núñez, L., Balbinot, E., Balog, Z., Barache, C., Barbato, D., Barros, M., Barstow, M.A., Bartolomé, S., Bassilana, J.L., Bauchet, N., Becciani, U., Bellazzini, M., Berihuete, A., Bernet, M., Bertone, S., Bianchi, L., Binnenfeld, A., Blanco-Cuaresma, S., Blazere, A., Boch, T., Bombrun, A., Bossini, D., Bouquillon, S., Bragaglia, A., Bramante, L., Breedt, E., Bressan, A., Brouillet, N., Brugaletta, E., Bucciarelli, B., Burlacu, A., Butkevich, A.G., Buzzi, R., Caffau, E., Cancelliere, R., Cantat-Gaudin, T., Carballo, R., Carlucci, T., Carnerero, M.I., Carrasco, J.M., Casamiquela, L., Castellani, M., Castro-Ginard, A., Chaoul, L., Charlot, P., Chemin, L., Chiaramida, V., Chiavassa, A., Chornay, N., Comoretto, G., Contursi, G., Cooper, W.J., Cornez, T., Cowell, S., Crifo, F., Cropper, M., Crosta, M., Crowley, C., Dafonte, C., Dapergolas, A., David, M., David, P., de Laverny, P., De Luise, F., De March, R., De Ridder, J., de Souza, R., de Torres, A., del Peloso, E.F., del Pozo, E., Delbo, M., Delgado, A., Delisle, J.B., Demouchy, C., Dharmawardena, T.E., Di Matteo, P., Diakite, S., Diener, C., Distefano, E., Dolding, C., Edvardsson, B., Enke, H., Fabre, C., Fabrizio, M., Faigler, S., Fedorets, G., Fernique, P., Fienga, A., Figueras, F., Fournier, Y., Fouron, C., Fragkoudi, F., Gai, M., Garcia-Gutierrez, A., Garcia-Reinaldos, M., García-Torres, M., Garofalo, A., Gavel, A., Gavras, P., Gerlach, E., Geyer, R., Giacobbe, P., Gilmore, G., Girona, S., Giuffrida, G., Gomel, R., Gomez, A., González-Núñez, J., González-Santamaría, I., González-Vidal, J.J., Granvik, M., Guillout, P., Guiraud, J., Gutiérrez-Sánchez, R., Guy, L.P., Hatzidimitriou, D., Hauser, M., Haywood, M., Helmer, A., Helmi, A., Sarmiento, M.H., Hidalgo, S.L., Hilger, T., Hładczuk, N., Hobbs, D., Holland, G.,

Huckle, H.E., Jardine, K., Jasniewicz, G., Jean-Antoine Piccolo, A., Jiménez-Arranz, Ó., Jorissen, A., Juaristi Campillo, J., Julbe, F., Karbevska, L., Kervella, P., Khanna, S., Kontizas, M., Kordopatis, G., Korn, A.J., Kóspál, Á., Kostrzewa-Rutkowska, Z., Kruszyńska, K., Kun, M., Laizeau, P., Lambert, S., Lanza, A.F., Lasne, Y., Le Campion, J.F., Lebreton, Y., Lebzelter, T., Leccia, S., Leclerc, N., Lecoeur-Taibi, I., Liao, S., Licata, E.L., Lindstrøm, H.E.P., Lister, T.A., Livanou, E., Lobel, A., Lorca, A., Loup, C., Madrero Pardo, P., Magdaleno Romeo, A., Managau, S., Mann, R.G., Manteiga, M., Marchant, J.M., Marconi, M., Marcos, J., Marcos Santos, M.M.S., Marín Pina, D., Marinoni, S., Marocco, F., Marshall, D.J., Martin Polo, L., Martín-Fleitas, J.M., Marton, G., Mary, N., Masip, A., Massari, D., Mastrobuono-Battisti, A., Mazeh, T., McMillan, P.J., Messina, S., Michalik, D., Millar, N.R., Mints, A., Molina, D., Molinaro, R., Molnár, L., Monari, G., Monguió, M., Montegriffo, P., Montero, A., Mor, R., Mora, A., Morbidelli, R., Morel, T., Morris, D., Muraveva, T., Murphy, C.P., Musella, I., Nagy, Z., Noval, L., Ocaña, F., Ogden, A., Ordenovic, C., Osinde, J.O., Pagani, C., Pagano, I., Palaversa, L., Palicio, P.A., Pallas-Quintela, L., Panahi, A., Payne-Wardenaar, S., Peñalosa Esteller, X., Penttilä, A., Pichon, B., Piersimoni, A.M., Pineau, F.X., Plachy, E., Plum, G., Poggio, E., Prša, A., Pulone, L., Racero, E., Ragaini, S., Rainer, M., Raiteri, C.M., Rambaux, N., Ramos, P., Ramos-Lerate, M., Re Fiorentin, P., Regibo, S., Richards, P.J., Rios Diaz, C., Ripepi, V., Riva, A., Rix, H.W., Rixon, G., Robichon, N., Robin, A.C., Robin, C., Roelens, M., Rogues, H.R.O., Rohrbasser, L., Romero-Gómez, M., Rowell, N., Royer, F., Mieres, D.Ruz., Rybicki, K.A., Sadowski, G., Sáez Núñez, A., Sagristà Sellés, A., Sahlmann, J., Salguero, E., Samaras, N., Sanchez Gimenez, V., Sanna, N., Santoveña, R., Sarasso, M., Schultheis, M., Sciacca, E., Segol, M., Segovia, J.C., Ségransan, D., Semeux, D., Shahaf, S., Siddiqui, H.I., Siebert, A., Siltala, L., Silvelo, A., Slezak, E., Slezak, I., Smart, R.L., Snaith, O.N., Solano, E., Solitro, F., Souami, D., Souchay, J., Spagna, A., Spina, L., Spoto, F., Steele, I.A., Steidelmüller, H., Stephenson, C.A., Süveges, M., Surdej, J., Szabados, L., Szegedi-Elek, E., Taris, F., Taylor, M.B., Teixeira, R., Tolomei, L., Tonello, N., Torra, F., Torra, J., Torralba Elipe, G., Trabucchi, M., Tsounis, A.T., Turon, C., Ulla, A., Unger, N., Vaillant, M.V., van Dillen, E., van Reeven, W., Vanel, O., Vecchiato, A., Viala, Y., Vicente, D., Voutsinas, S., Weiler, M., Wevers, T., Wyrzykowski, Ł., Yoldas, A., Yvard, P., Zhao, H., Zorec, J., Zucker, S., Zwitter, T., 2023. Gaia data release 3. Summary of the content and survey properties. Astron. Astrophys. 674, 1. http://dx.doi.org/10.1051/0004-6361/202243940, arXiv:2208.00211.

Gilliland, R.L., Brown, T.M., Christensen-Dalsgaard, J., Kjeldsen, H., Aerts, C., Appourchaux, T., Basu, S., Bedding, T.R., Chaplin, W.J., Cunha, M.S., De Cat, P., De Ridder, J., Guzik, J.A., Handler, G., Kawaler, S., Kiss, L., Kolenberg, K., Kurtz, D.W., Metcalfe, T.S., Monteiro, M.J.P.F.G., Szabó, R., Arentoft, T., Balona, L., Debosscher, J., Elsworth, Y.P., Quirion, P.O., Stello, D., Suárez, J.C., Borucki, W.J., Jenkins, J.M., Koch, D., Kondo, Y., Latham, D.W., Rowe, J.F., Steffen, J.H., 2010. Kepler asteroseismology program: Introduction and first results. Publ. Astron. Soc. Pac. 122, 131. http://dx.doi.org/10.1086/650399, arXiv:1001.0139.

Ginsburg, A., Sipőcz, B.M., Brasseur, C.E., Cowperthwaite, P.S., Craig, M.W., Deil, C., Guillochon, J., Guzman, G., Liedtke, S., Lian Lim, P., Lockhart, K.E., Mommert, M., Morris, B.M., Norman, H., Parikh, M., Persson, M.V., Robitaille, T.P., Segovia, J.C., Singer, L.P., Tollerud, E.J., de Val-Borro, M., Valtchanov, I., Woillez, J., Astroquery Collaboration, a subset of astropy Collaboration, 2019. Astroquery: An astronomical web-querying package in python. Astron. J. 157, 98. http://dx.doi.org/10.3847/1538-3881/aafc33, arXiv:1901.04520.

Guerrero, N.M., Seager, S., Huang, C.X., Vanderburg, A., Garcia Soto, A., Mireles, I., Hesse, K., Fong, W., Glidden, A., Shporer, A., Latham, D.W., Collins, K.A., Quinn, S.N., Burt, J., Dragomir, D., Crossfield, I., Vanderspek, R., Fausnaugh, M., Burke, C.J., Ricker, G., Daylan, T., Essack, Z., Günther, M.N., Osborn, H.P., Pepper, J., Rowden, P., Sha, L., Villanueva Steven, J., Yahalomi, D.A., Yu, L., Ballard, S., Batalha, N.M., Berardo, D., Chontos, A., Dittmann, J.A., Esquerdo, G.A., Mikal-Evans, T., Jayaraman, R., Krishnamurthy, A., Louie, D.R., Mehrle, N., Niraula, P., Rackham, B.V., Rodriguez, J.E., Rowden, S.J.L., Sousa-Silva, C., Watanabe, D., Wong, I., Zhan, Z., Zivanovic, G., Christiansen, J.L., Ciardi, D.R., Swain, M.A., Lund, M.B., Mullally, S.E., Fleming, S.W., Rodriguez, D.R., Boyd, P.T., Quintana, E.V., Barclay, T., Colón, K.D., Rinehart, S.A., Schlieder, J.E., Clampin, M., Jenkins, J.M., Twicken, J.D., Caldwell, D.A., Coughlin, J.L., Henze, C., Lissauer, J.J., Morris, R.L., Rose, M.E., Smith, J.C., Tenenbaum, P., Ting, E.B., Wohler, B., Bakos, G.Á., Bean, J.L., Berta-Thompson, Z.K., Bieryla, A., Bouma, L.G., Buchhave, L.A., Butler, N., Charbonneau, D., Doty, J.P., Ge, J., Holman, M.J., Howard, A.W., Kaltenegger, L., Kane, S.R., Kjeldsen, H., Kreidberg, L., Lin, D.N.C., Minsky, C., Narita, N., Paegert, M., Pál, A., Palle, E., Sasselov, D.D., Spencer, A., Sozzetti, A., Stassun, K.G., Torres, G., Udry, S., Winn, J.N., 2021. The TESS objects of interest catalog from the TESS prime mission. Astrophys. J. Suppl. 254, 39. http://dx.doi.org/10.3847/1538-4365/abefe1, arXiv:2103.12538.

Guzik, J.A., Kaye, A.B., Bradley, P.A., Cox, A.N., Neuforge, C., 2000. Driving the gravity-mode pulsations in γ Doradus variables. Astrophys. J. Lett. 542, L57–L60. http://dx.doi.org/10.1086/312908.

Handler, G., Meingast, S., 2011. New β Cephei stars in the young open cluster NGC 637. Astron. Astrophys. 533, 70. http://dx.doi.org/10.1051/0004-6361/201116874, arXiv:1105.3121.

Handler, G., Shobbrook, R.R., 2002. On the relationship between the δ Scuti and γ Doradus pulsators. Mon. Not. R. Astron. Soc. 333, 251–262. http://dx.doi.org/10.1046/j.1365-8711.2002.05401.x, arXiv:astro-ph/0202152.

Harris, C.R., Millman, K.J., van der Walt, S.J., Gommers, R., Virtanen, P., Cournapeau, D., Wieser, E., Taylor, J., Berg, S., Smith, N.J., Kern, R., Picus, M., Hoyer, S., van Kerkwijk, M.H., Brett, M., Haldane, A., del Río, J.F., Wiebe, M., Peterson, P., Gérard-Marchant, P., Sheppard, K., Reddy, T., Weckesser, W., Abbasi, H., Gohlke, C., Oliphant, T.E., 2020. Array programming with NumPy. Nature 585, 357–362. http://dx.doi.org/10.1038/s41586-020-2649-2.

Hill, K.L., Littlefield, C., Garnavich, P., Scaringi, S., Szkody, P., Mason, P.A., Kennedy, M.R., Shaw, A.W., Covington, A.E., 2022. Hitting a new low: The unique 28 hr cessation of accretion in the TESS light curve of YY dra (DO dra). Astron. J. 163, 246. http://dx.doi.org/10.3847/1538-3881/ac5a51, arXiv:2203.00221.

Hon, M., Huber, D., Kuszlewicz, J.S., Stello, D., Sharma, S., Tayar, J., Zinn, J.C., Vrard, M., Pinsonneault, M.H., 2021. A quick look at all-sky galactic archeology with TESS: 158 000 oscillating red giants from the MIT quick-look pipeline. Astrophys. J. 919, 131. http://dx.doi.org/10.3847/1538-4357/ac14b1, arXiv:2108.01241.

Howell, S.B., Sobeck, C., Haas, M., Still, M., Barclay, T., Mullally, F., Troeltzsch, J., Aigrain, S., Bryson, S.T., Caldwell, D., Chaplin, W.J., Cochran, W.D., Huber, D., Marcy, G.W., Miglio, A., Najita, J.R., Smith, M., Twicken, J.D., Fortney, J.J., 2014. The K2 mission: Characterization and early results. Publ. Astron. Soc. Pac. 126, 398. http://dx.doi.org/10.1086/676406, arXiv:1402.5163.

Hunter, J.D., 2007. Matplotlib: A 2d graphics environment. Comput. Sci. Eng. 9, 90–95. http://dx.doi.org/10.1109/MCSE.2007.55.

Kazarovets, E.V., Samus, N.N., Durlevich, O.V., Kireeva, N.N., Pastukhova, E.N., 2015. The 81st name-list of variable stars. Part I - RA 00h to 17h30. Inf. Bull. Var. Stars 6151, 1.

Khruslov, A.V., 2010. Multiperiodic Delta Scuti variables with nonradial pulsations. Perem. Zvezdy Prilozhenie 10, 15.

Kiss, L.L., Alfaro, E.J., Bakos, G., Csak, B., Szatmary, K., 1999a. On the monoperiodicity of the suspected delta Scuti star Iota Bootis. Inf. Bull. Var. Stars 4698, 1.

Kiss, L.L., Alfaro, E.J., Bakos, G., Csak, B., Szatmary, K., 1999b. On the monoperiodicity of the suspected delta Scuti star Iota Bootis. Inf. Bull. Var. Stars 4698, 1.

Lenz, P., Breger, M., 2005. Period04 user guide. Commun. Asteroseismol. 146, 53–136. http://dx.doi.org/10.1553/cia146s53.

Liakos, A., Niarchos, P., 2017. Catalogue and properties of δ Scuti stars in binaries. Mon. Not. R. Astron. Soc. 465, 1181–1200. http://dx.doi.org/10.1093/mnras/stw2756, arXiv:1611.00200.

Lightkurve Collaboration, Cardoso, J.V.d.M., Hedges, C., Gully-Santiago, M., Saunders, N., Cody, A.M., Barclay, T., Hall, O., Sagear, S., Turtelboom, E., Zhang, J., Tzanidakis, A., Mighell, K., Coughlin, J., Bell, K., Berta-Thompson, Z., Williams, P., Dotson, J., Barentsen, G., 2018. Lightkurve: Kepler and TESS time series analysis in Python. Astrophys. Source Code Libr. arXiv:1812.013.

Littlefield, C., Scaringi, S., Garnavich, P., Szkody, P., Kennedy, M.R., Iłkiewicz, K., Mason, P.A., 2021. Quasi-periodic oscillations in the TESS light curve of TX col, a diskless intermediate polar on the precipice of forming an accretion disk. Astron. J 162, 49. http://dx.doi.org/10.3847/1538-3881/ac062b, arXiv:2104.14140.

Liu, Z.L., Jiang, S.Y., Zhou, A.Y., Liu, Y.Y., Li, Z.P., Men, L., Li, H.B., 1998. A new delta scuti variable star - SAO 16394. Inf. Bull. Var. Stars 4592, 1.

Liu, Z.L., Zhou, A.Y., Rodríguez, E., 2000. The mode identification and physical parameter determination of the delta Scuti star SAO 16394. Astron. Astrophys. 362, 1041–1045.

Mason, B.D., Wycoff, G.L., Hartkopf, W.I., Douglass, G.G., Worley, C.E., 2001. The 2001 US naval observatory double star CD-ROM. I. The washington double star catalog. Astron. J. 122, 3466–3471. http://dx.doi.org/10.1086/323920.

Paegert, M., Stassun, K.G., Collins, K.A., Pepper, J., Torres, G., Jenkins, J., Twicken, J.D., Latham, D.W., 2021. TESS input catalog versions 8.1 and 8.2: Phantoms in the 8.0 catalog and how to handle them. arXiv e-prints, arXiv:2108.04778, arXiv:2108.04778.

Pamos Ortega, D., García Hernández, A., Suárez, J.C., Pascual Granado, J., Barceló Forteza, S., Rodón, J.R., 2022. Determining the seismic age of the young open cluster α Per using δ Scuti stars. Mon. Not. R. Astron. Soc. 513, 374–388. http://dx.doi.org/10.1093/mnras/stac864, arXiv:2203.14256.

Pamos Ortega, D., Mirouh, G.M., García Hernández, A., Suárez Yanes, J.C., Barceló Forteza, S., 2023. Dating young open clusters using δ Scuti stars. Results for Trumpler 10 and Praesepe. Astron. Astrophys. 675, 167. http://dx.doi.org/10.1051/0004-6361/202346323, arXiv:2306.02791.

Perez Hernandez, F., Claret, A., Belmonte, J.A., 1995. Pulsation in moderate rotating δ Scuti stars: the case of BN and BU Cancri. Astron. Astrophys. 295, 113–122.

Pojmanski, G., 2002. The all sky automated survey. Catalog of variable stars. I. 0 h - 6 hQuarter of the Southern Hemisphere. Acta Astron. 52, 397–427, arXiv:astro-ph/0210283.

Prša, A., Kochoska, A., Conroy, K.E., Eisner, N., Hey, D.R., IJspeert, L., Kruse, E., Fleming, S.W., Johnston, C., Kristiansen, M.H., LaCourse, D., Mortensen, D., Pepper, J., Stassun, K.G., Torres, G., Abdul-Masih, M., Chakraborty, J., Gagliano, R., Guo, Z., Hambleton, K., Hong, K., Jacobs, T., Jones, D., Kostov, V., Lee, J.W., Omohundro, M., Orosz, J.A., Page, E.J., Powell, B.P., Rappaport, S., Reed, P., Schnittman, J., Schwengeler, H.M., Shporer, A., Terentev, I.A., Vanderburg, A., Welsh, W.F., Caldwell, D.A., Doty, J.P., Jenkins, J.M., Latham, D.W., Ricker, G.R., Seager, S., Schlieder, J.E., Shiao, B., Vanderspek, R., Winn, J.N., 2022. TESS eclipsing binary stars. I. Short-cadence observations of 4584 eclipsing binaries in sectors 1-26. Astrophys. J. Suppl. 258, 16. http://dx.doi.org/10.3847/1538-4365/ac324a, arXiv:2110.13382.

Ricker, G.R., Winn, J.N., Vanderspek, R., Latham, D.W., Bakos, G.Á., Bean, J.L., Berta-Thompson, Z.K., Brown, T.M., Buchhave, L., Butler, N.R., Butler, R.P., Chaplin, W.J., Charbonneau, D., Christensen-Dalsgaard, J., Clampin, M., Deming, D., Doty, J., De Lee, N., Dressing, C., Dunham, E.W., Endl, M., Fressin, F., Ge, J.,

Henning, T., Holman, M.J., Howard, A.W., Ida, S., Jenkins, J.M., Jernigan, G., Johnson, J.A., Kaltenegger, L., Kawai, N., Kjeldsen, H., Laughlin, G., Levine, A.M., Lin, D., Lissauer, J.J., MacQueen, P., Marcy, G., McCullough, P.R., Morton, T.D., Narita, N., Paegert, M., Palle, E., Pepe, F., Pepper, J., Quirrenbach, A., Rinehart, S.A., Sasselov, D., Sato, B., Seager, S., Sozzetti, A., Stassun, K.G., Sullivan, P., Szentgyorgyi, A., Torres, G., Udry, S., Villasenor, J., 2015. Transiting Exoplanet Survey Satellite (TESS). J. Astron. Telesc., Instrum., Syst. 1, 014003. http://dx.doi.org/10.1117/1.JATIS.1.1.014003.

Rodríguez, E., López-González, M.J., López de Coca, P., 2000. A revised catalogue of delta Sct stars. Astron. Astrophys. 144, 469–474. http://dx.doi.org/10.1051/aas:2000221.

Sangaralingam, V., Stevens, I.R., 2011. STEREO TRansiting Exoplanet and Stellar Survey (STRESS) - I. Introduction and data pipeline. Mon. Not. R. Astron. Soc. 418, 1325–1334. http://dx.doi.org/10.1111/j.1365-2966.2011.19581.x.

Stassun, K.G., Oelkers, R.J., Pepper, J., Paegert, M., De Lee, N., Torres, G., Latham, D.W., Charpinet, S., Dressing, C.D., Huber, D., Kane, S.R., Lépine, S., Mann, A., Muirhead, P.S., Rojas-Ayala, B., Silvotti, R., Fleming, S.W., Levine, A., Plavchan, P., 2018. The TESS input catalog and candidate Target List. Astron. J. 156, 102. http://dx.doi.org/10.3847/1538-3881/aad050, arXiv:1706.00495.

Steindl, T., Zwintz, K., Bowman, D.M., 2021. Tidally perturbed pulsations in the pre-main sequence δ Scuti binary RS Cha. Astron. Astrophys. 645, A119. http://dx.doi.org/10.1051/0004-6361/202039093, arXiv:2011.08214.

The Astropy Collaboration, Price-Whelan, A.M., Sipőcz, B.M., Günther, H.M., Lim, P.L., Crawford, S.M., Conseil, S., Shupe, D.L., Craig, M.W., Dencheva, N., Ginsburg, A., VanderPlas, J.T., Bradley, L.D., Pérez-Suárez, D., de Val-Borro, M., Paper Contributors, Aldcroft, T.L., Cruz, K.L., Robitaille, T.P., Tollerud, E.J., Coordination Committee, Ardelean, C., Babej, T., Bach, Y.P., Bachetti, M., Bakanov, A.V., Bamford, S.P., Barentsen, G., Barmby, P., Baumbach, A., Berry, K.L., Biscani, F., Boquien, M., Bostroem, K.A., Bouma, L.G., Brammer, G.B., Bray, E.M., Breytenbach, H., Buddelmeijer, H., Burke, D.J., Calderone, G., Cano Rodríguez, J.L., Cara, M., Cardoso, J.V.M., Cheedella, S., Copin, Y., Corrales, L., Crichton, D., D'Avella, D., Deil, C., Depagne, É., Dietrich, J.P., Donath, A., Droettboom, M., Earl, N., Erben, T., Fabbro, S., Ferreira, L.A., Finethy, T., Fox, R.T., Garrison, L.H., Gibbons, S.L.J., Goldstein, D.A., Gommers, R., Greco, J.P., Greenfield, P., Groener, A.M., Grollier, F., Hagen, A., Hirst, P., Homeier, D., Horton, A.J., Hosseinzadeh, G., Hu, L., Hunkeler, J.S., Ivezić, Ž., Jain, A., Jenness, T., Kanarek, G., Kendrew, S., Kern, N.S., Kerzendorf, W.E., Khvalko, A., King, J., Kirkby, D., Kulkarni, A.M., Kumar, A., Lee, A., Lenz, D., Littlefair, S.P., Ma, Z., Macleod, D.M., Mastropietro, M., McCully, C., Montagnac, S., Morris, B.M., Mueller, M., Mumford, S.J., Muna, D., Murphy, N.A., Nelson, S., Nguyen, G.H., Ninan, J.P., Nöthe, M., Ogaz, S., Oh, S., Parejko, J.K., Parley, N., Pascual, S., Patil, R., Patil, A.A., Plunkett, A.L., Prochaska, J.X., Rastogi, T., Reddy Janga, V., Sabater, J., Sakurikar, P., Seifert, M., Sherbert, L.E., Sherwood-Taylor, H., Shih, A.Y., Sick, J., Silbiger, M.T., Singanamalla, S., Singer, L.P., Sladen, P.H., Sooley, K.A., Sornarajah, S., Streicher, O., Teuben, P., Thomas, S.W., Tremblay, G.R., Turner, J.E.H., Terrón, V., van Kerkwijk, M.H., de la Vega, A., Watkins, L.L., Weaver, B.A., Whitmore, J.B., Woillez, J., Zabalza, V., Contributors, 2018. The astropy project: Building an open-science project and status of the v2.0 core package. Astron. J. 156, 123. http://dx.doi.org/10.3847/1538-3881/aabc4f, arXiv:1801.02634.

Virtanen, P., Gommers, R., Oliphant, T.E., Haberland, M., Reddy, T., Cournapeau, D., Burovski, E., Peterson, P., Weckesser, W., Bright, J., van der Walt, S.J., Brett, M., Wilson, J., Millman, K.J., Mayorov, N., Nelson, A.R.J., Jones, E., Kern, R., Larson, E., Carey, C.J., Polat, İ., Feng, Y., Moore, E.W., VanderPlas, J., Laxalde, D., Perktold, J., Cimrman, R., Henriksen, I., Quintero, E.A., Harris, C.R., Archibald, A.M., Ribeiro, A.H., Pedregosa, F., van Mulbregt, P., SciPy 1.0 Contributors, 2020. SciPy 1.0: Fundamental algorithms for scientific computing in python. Nature Methods 17, 261–272. http://dx.doi.org/10.1038/s41592-019-0686-2.

von Essen, C., Mallonn, M., Borre, C.C., Antoci, V., Stassun, K.G., Khalafinejad, S., Tautvaišene, G., 2020. TESS unveils the phase curve of WASP-33b. Characterization of the planetary atmosphere and the pulsations from the star. Astron. Astrophys. 639, A34. http://dx.doi.org/10.1051/0004-6361/202037905, arXiv:2004.10767.

Xiong, D.R., Deng, L., Zhang, C., Wang, K., 2016. Turbulent convection and pulsation stability of stars - II. Theoretical instability strip for δ Scuti and γ Doradus stars. Mon. Not. R. Astron. Soc. 457, 3163–3177. http://dx.doi.org/10.1093/mnras/stw047, arXiv:1808.09621.

Yakut, K., Zima, W., Kalomeni, B., van Winckel, H., Waelkens, C., De Cat, P., Bauwens, E., Vučković, M., Saesen, S., Le Guillou, L., Parmaksızoğlu, M., Uluç, K., Khamitov, I., Raskin, G., Aerts, C., 2009. Close binary and other variable stars in the solar-age Galactic open cluster M 67. Astron. Astrophys. 503, 165–176. http://dx.doi.org/10.1051/0004-6361/200911918, arXiv:0906.4908.

Zhang, X.B., Zhang, R.X., Li, Z.P., 2005. S1280 and S1284: Two oscillating blue stragglers in the open cluster M67. Chin. J. Astron. Astrophys. 5, 579–586. http://dx.doi.org/10.1088/1009-9271/5/6/003.

Zhou, A.Y., 1999. The single frequency solution of the delta scuti star τ boo. Delta Scuti Star Newsl. 13, 7.

Zhou, A.Y., 2001. CCD photometry of the field of EX cancri. Inf. Bull. Var. Stars 5096, 1.

Zhou, A.Y., 2002. Photometry of δ sct-type and related stars: Results of AD ari, IP vir and YZ boo. Chin. J. Astron. Astrophys. 2, 43–50. http://dx.doi.org/10.1088/1009-9271/2/1/43.

Zhou, A.Y., 2024. Unveiling δ Scuti and γ Doradus hybrid pulsation of HD 53166 and HD 53349 plus rich frequencies in HD 52788. New Astron. 105, 102081. http://dx.doi.org/10.1016/j.newast.2023.102081, arXiv:2301.08355.

Zhou, A.Y., Liu, Z.L., Du, B.T., 2001a. Bi-modal pulsation of the delta Scuti star V1821 Cygni. Astron. Astrophys. 371, 233–239. http://dx.doi.org/10.1051/0004-6361:20010375.

Zhou, A.Y., Rodríguez, E., Liu, Z.L., Du, B.T., 2001b. Multiperiodicity and physical nature of the δ Sct star GSC 2683-3076. Mon. Not. R. Astron. Soc. 326, 317–325. http://dx.doi.org/10.1046/j.1365-8711.2001.04604.x.

Zhou, A.Y., Rodríguez, E., Rolland, A., Costa, V., 2001c. Photometric properties of the δ Scuti star BR Cancri. Mon. Not. R. Astron. Soc. 323, 923–929. http://dx.doi.org/10.1046/j.1365-8711.2001.04275.x.

Ziaali, E., Bedding, T.R., Murphy, S.J., Van Reeth, T., Hey, D.R., 2019. The period-luminosity relation for δ Scuti stars using Gaia DR2 parallaxes. Mon. Not. R. Astron. Soc. 486, 4348–4353. http://dx.doi.org/10.1093/mnras/stz1110, arXiv:1904.08101.